‘Doppler’ Cooling in high-T_c Superconductors

Submitted in partial fulfilment of the requirements for the degree of Masters by Research



Muhammad Zoubeir Khan Emambokus

Balliol College

Trinity Term 2015

Abstract

Thanks to growing capibilities in modulating the properties of materials by selectively driving a specific degree of freedom, along with recent developments in terahertz science, it has been possible to excite and probe the Josephson mode in cuprate superconductors. It is believed that in these materials, phase fluctuations in the superconducting order parameter, which are manifested by Josephson plasmonic excitations can be important in determining the critical temperature. Current efforts in finding novel ways of enhancing superconductivity are geared towards developing ways of using coherent control of this phase to reduce thermal fluctuations, hence improving the effective critical temperature in such materials.

With this in view, we propose a 'Doppler' Cooling scheme for layered superconductors having a bilayer structure and conduct a feasibility study to assess their applicability to such systems. By modelling a bilayer cuprate unit-cell as two coupled Joesphson junctions, we find that it is possible to induce transitions between and interlayer and higher energy intralayer plasmonic mode via driving from an externally applied electromagnetic field only when the junction is current biased. Our study shows that the physics of the system allow such a scheme to be implemented. The low recoil imparted by photons at terahertz frequencies enables us to apply the same framework as for cooling of atomic systems. The relatively long lifetimes (~ 0.1 ns) against spontaneous decay estimated imply that cooling is not likely to be limited by inherent features of the scheme but will rather depend on other factors, such as the competition between cooling and rethermalisation. These factors need to be further studied to assess the experimental viability of the proposed scheme.

Contents

1 Introduction **3**

1.1 The quest for a room temperature superconductor 3

1.2 Selective dynamical control 4

1.3 Thesis outline 7

2 Terahertz technology and recent progress **8**

2.1 Overview of Terahertz generation methods 9

2.2 Photoconduction and optical rectification 12

2.3 Free Electron Lasers 14

2.4 Quantum Cascade Lasers 18

3 Laser cooling in atomic systems **22**

3.1 Atom-light interaction 23

3.2 Doppler cooling 31

3.3 Sub-Doppler cooling 38

4 High T_c Superconductors and Josephson Physics **41**

4.1 High T_c Superconductors 41

4.1.1 Introduction and overview of superconductivity 41

4.1.2 The London Equations 47

4.1.3 Ginzburg-Landau Theory 48

4.1.4 More on HTS and Cuprates 52
4.2 Josephson Physics 58
4.2.1 Origin of the Josephson effect 59
4.2.2 Phase cooling 63
4.2.3 Long Junctions 66

5 A Doppler Cooling Scheme for bilayer cuprates 69
5.1 The model 69
5.2 'Doppler' cooling scheme 75
5.3 Driving transitions 77
5.4 Doppler cooling limit 80
5.5 Validity of the treatment 82
5.6 Reheating 83

6 Summary and Outlook 85

Chapter 1

Introduction

1.1 The quest for a room temperature superconductor

The discovery by Bednorz and Müller of superconductivity at above what was thought to be a theoretical limit of $\sim$ 30 K [1, 2] sparked renewed efforts to find materials of ever higher critical temperatures (T_c): the temperature below which a material exhibits superconductive properties such as perfect conductivity and diamagnetism [3]. Before the groundbreaking discovery, research to find high-temperature superconductors was limited [4] since there had been growing skepticism within the scientific community of ever breaking the limit realistically achievable in superconducting materials [2], which were all thought to display superconductivity as a result of the weak electron-phonon coupling mechanisms explained by BCS theory [5]. Indeed the highest achieved critical temperature before Bednorz's discovery was 22 K, in Nb-Ge films and had been so for 13 years with no improvement [6, 7].

A later observation of the superconducting transition at 93 K in yttrium bar-

ium copper oxide (YBCO) [8] suddenly revived hopes for practical applications of superconductivity as this new material could be cooled with the much cheaper and abundantly available liquid nitrogen (boiling point 77 K) instead of the traditional liquid helium, thus making any application more economically viable. The big strides in increasing T_c renewed ideas about whether materials could be made to superconduct without any refrigeration [3].

YBCO along with the superconductor discovered by Bednorz belong to a class of materials called cuprates. They are in fact Mott insulators which become superconducting as they are doped. A logical route to increase T_c was to vary the chemical composition and levels of doping to find an optimised formulation. In cuprates, the critical temperature typically increases with higher levels of doping until a maximum after which any further doping will reduce T_c (see for example figure 4.3 in Chapter 4). The highest T_c achieved by this method was about 135 K in optimally doped mercury barium calcium copper oxide systems [10]. Other avenues have been explored in an attempt to further enhance superconductivity. Application of high pressures on cuprates have enabled an increase in T_c of up to around 165 K [2,11]. Recently a record of 203 K was reported in the BCS type sulphur hydride system [12]. The use of magnetic fields has also been demonstrated to enhance effective critical temperatures [13–15]. However these conventional methods have so far been unable to produce a room temperature superconductor and this 'Holy Grail' of superconductivity still remains elusive today.

1.2 Selective dynamical control

As will be discussed in Chapter 4, cuprate superconductors are made up of copper oxide layers, believed to the superconducting component in the crystal structure These are separated by generally thicker insulating layers. Charge transport across

the oxide layers (c-axis transport) is largely governed by Jospehson tunneling (see Chapter 5) and unlike in conventional superconductors loss of phase coherence, via quantum or thermal fluctuations can be an important factor in destroying superconductivity, especially in underdoped compounds (Chapter 4). A new area of research is developing to find ways of optimizing superconductivity in these materials by directly targeting these thermal phase fluctuations which are manifested by Josephson plasmonic excitations, thereby increasing their effective critical temperature. These Josephson excitations are typically within the terahertz energy range in the cuprates.

The use of light to modulate electronic properties and crystal structures (for example via the excitation of phonon modes) of materials has gained increasing interest in research as well as for technological applications [16]. A considerable amount of work has been carried out in this area using optical frequencies, revealing remarkable results such as photo-induced insulator to metal transitions in manganites [17] or organic salts [18]. Excitation at such high frequencies can be highly incoherent, poorly selective in that many degrees of freedom are simultaneously excited and typically induce heating [19]. In recent years however, the demonstration of phase control in matter by the coherent driving of a specific vibrational mode [20] has opened up new possibilities for material control. One of the most notable observations of this highly selective phononic driving, which often lies in the mid-infrared region and typically induces little direct heating [16] has been transient light induced superconductivity in stripe-ordered cuprates [21–23]. More interesting and relevant to this work, has been the demonstration of selective excitation of Josephson plasma resonances in cuprates [24, 25], which along with the developments in terahertz technology (Chapter 2) support the phase cooling approach mentioned above as a realisable proposal with current technological capabilities in experimental physics, with good prospects for commercial applications

given the advancements being made in terahertz sources (Chapter 2).

Current efforts towards an experimental realization of this selective dynamical control approach are centered on developing laser or cavity cooling schemes, importing and adapting ideas from laser/cavity cooling of atoms (see Chapter 3) and optomechanical devices [26]. Phase cooling by driving has been experimentally demonstrated in a single extended Josephson junction made of a BCS superconductor [27], employing in essence a sideband cooling scheme. The authors were able to measure an enhancement in the critical current, a sign of reduced phase fluctuations (see Chapter 5). Recently Denny *et al.* proposed a parametric cooling scheme applicable to short junctions [16]. The scheme is based on the selective driving of a c-axis vibrational mode, which amounts to a modulation of the coupling between two modes of Josephson plasma oscillations (phase oscillation modes) allowing the exchange of energy between them. This allows the lower energy, thermally excited mode to be depopulated, thereby reducing phase fluctuations.

In this thesis we propose a Doppler cooling scheme for two non-identical inductively and capacitively coupled long Josephson junctions, with a view of applying the technique to layered superconductors exhibiting a bilayer structure like YBCO. In essence, the Doppler cooling mechanism reduces and restricts phase fluctuations in long junctions so that, ideally, they are uniform along the length of the junction, hence effectively reducing the system to the short junction limit considered by Denny *et al.* The work presented in this thesis is therefore envisaged as an additional stage in the cooling process of extended samples, whereby 'Doppler' cooling would first be applied, effectively reducing the system to a one-dimensional one, followed by the parametric cooling designed for short junctions.

1.3 Thesis outline

The thesis is organised as follows. In Chapter 2 we review the technological progress made in terahertz science with a particular focus on terahertz sources: a crucial component for selectively driving Josephson excitations in layered superconductors and thus implement our proposed cooling scheme. Chapter 3 outlines the Doppler cooling mechanism in atomic systems and provides a template for developing a counterpart applicable to phase fluctuations in cuprate systems. Chapter 4 is split into two sections. In the first we present a brief overview of the development of superconductivity followed by a discussion of phenomenological descriptions of superconductivity like the London and Ginzburg-Landau theories which are key concepts in the framework we use to describe the electrodynamics in layered systems. A subsection is dedicated to the cuprate HTS where we argue, backed by past experimental evidence, the validity of a model for layered superconductors as stacks of coupled Josephson junctions and the importance of phase fluctuations in determining T_c in some materials. The Josephson physics required for constructing such a model is then outlined in the second section of the chapter. Chapter 5 is where we present the actual model, the cooling scheme and the results of our feasibility study. The thesis is concluded with a summary and a brief discussion for future work in Chapter 6.

Chapter 2

Terahertz technology and recent progress

Initially coined by spectroscopists [28] to refer to electromagnetic waves of frequency just below that of far infrared radiation, today, the term Terahertz is generally employed to designate radiation broadly within the range 0.1 THz to 10 THz, although definitions differ about the upper frequency limit. With a corresponding wavelength range between 3 mm to 30 μm, they are also referred to as submillimeter waves and occupy the gap between the microwave and infrared regions of the electromagnetic spectrum. Since conventional electronic devices used to generate and detect radio waves and microwaves cannot be operated at the higher terahertz frequencies and neither can well established optical setups typically employed for the infrared region be directly applied for lower frequencies, this region of the electromagnetic spectrum has for a long time lacked suitable sources and detectors, commonly known within engineering circles as the terahertz gap.

Yet any hope of future implementation of the research presented in this thesis requires sufficiently technologically advanced devices operating within the terahertz range. As mentioned in Chapter 1 and will be further discussed in Chapter 4, many

fundamental excitations in layered superconductors like phonon modes and more importantly the Josephson plasma resonance on which this research is centered occur at terahertz energies. Different types of terahertz sources are required at the various stages along the road to implementing this research. Femtosecond pulsed broadband and narrowband sources of sufficient power are needed to characterize superconducting samples and thus assess their suitability as possible candidates for use in proof of principle demonstrations. The most widely employed technique is time-domain spectroscopy [29–31]. Realizing the cooling scheme itself will require continuous wave sources offering a high level of tuning like fast enough frequency sweeps. Furthermore, any practical application of the laser cooling schemes will require adequately miniaturized THz components.

Motivated by the myriad of possible research and commercial applications of terahertz science and with the advent of breakthroughs in photonics and nanotechnology [32, 33], the last couple of decades have seen renewed efforts in the development of sub-millimetre devices, especially the terahertz source which has been the most difficult component to realise [28]. Today, a wide variety of methods are utilized to generate sub-millimetre waves. This chapter first gives an overview of the efforts towards developing terahertz sources, followed by further discussions on the most pertinent and promising approaches.

2.1 Overview of Terahertz generation methods

Terahertz emitting devices can be roughly categorised as pulsed broadband, continuous narrowband or incoherent sources. Only the first two types will be covered here. A first approach, which for a long time has been the most common route, involves modifying already well established solid-state electronic devices to extend their operable frequency range into the terahertz regime. Advances in nanotech-

nology brought about ever smaller high electron mobility transistors (HEMT's) of reduced gate capacitance and carrier transit times [34]. This enabled them to be developed into room temperature voltage-tuneable terahertz emitters and detectors [34–36]. Improved fabrication methods such as epitaxial growth techniques, nucleation and nanolithography have enabled more intricate novel designs of otherwise traditional microwave devices such as Gunn diodes with planar geometries to be proposed as sources [37]. Additionally, impact ionization avalanche transit-time diodes (IMPATT) which have been experimentally demonstrated as a source for W-band microwave radiation (75-100 GHz) [38] underwent theoretical investigations as prospective terahertz emitters. The performance limitations of double-drift region (DDR) IMPATTs based on various semiconductor materials have been studied and frequencies as high as 5 THz are expected from Wurtzite-GaN (Wz-GaN) DDR IMPATTs [39].

Yet another solid-state electronic approach involves upconverting microwave signals typically using a chain of planar GaAs Schottky-diode multipliers. Frequencies of up to 2.7 THz have been experimentally achieved [40] and more recently a tuneable frequency tripler spanning the range 2.4 to 2.7 THz has been demonstrated [41]. While the above solid state devices present the significant advantage of being compact and easily integrable into electronic circuits, they have so far only been able to reach the lower frequency end of the THz range. Furthermore their output power tends to decrease with increasing frequency meaning that while they can deliver milliwatts of power in the W-band, THz generation remains limited to microwatts [28].

Vacuum electronic THz sources on the other hand boast and impressive power (mw to GW) and frequency (0.1 to 10 THz) coverage, largely due to the free electron laser. These are large scale facilities that exploit the acceleration of electron beams to produce THz radiation. Free electron lasers can provide both continuous and

pulsed outputs of peak powers as high as 10^9 W spanning the whole terahertz range [42], making them ideal sources for applications such as non-linear terahertz spectroscopy. Their working principle is further discussed in section 2.3. Table top variations of free electron lasers, based on the same working principle also exist. These include the backward wave oscillator, the klystron and the travelling-wave tube. They are however not as widely used at present although they are still being developed and improved by some research groups [28, 42, 44–47]. Their operating frequency range is currently only 0.1 - 1.0 THz with output powers between 1 mW - 1 kW.

To date, downconversion from optical frequencies remains the most commercially successful technique for producing terahertz radiation [28]. Various schemes use visible or near infrared lasers like photomixing [48] where frequency offset lasers are used to induce a photocurrent in a semiconductor. The current is modulated at the laser difference frequency which falls in the THz range. It is then coupled to an antenna which radiates at that frequency. The method typically produces output powers of the order of microwatts at frequencies of about 3 THz. Other examples include optical parametric oscillators [49] or generation via photoionization of gases [50]. However, the most widespread methods for generating pulsed broadband outputs, useful in terahertz time-domain spectroscopy are optical rectification [55] and photoconduction [51] and are further discussed in section 2.2.

The method having received the most attention over the past decade and which has now emerged as the most promising candidate terahertz source is the quantum cascade laser (QCL). The technique, based on intersubband transitions in quantum well heterostructures proposed in 1971 [57] was first demonstrated in the infrared region at an operating wavelength of 4.2 μm with peak powers above 8 mW [59]. Difficulties due to the long wavelength of terahertz radiation had prevented the realisation of QCLs operating in this regime. These include the poor coupling

between the small gain medium and the optical mode and significant losses due to stronger absorption at longer wavelengths by free electrons in the material. They were finally overcome by Kohler *et al.* [59] who used new design involving a chirped superlattice and more sophisticated double-plasmon structure waveguides. Laser operation was demonstrated at 4.4 THz with output powers exceeding 2 mW. There has since been considerable effort to increase the frequency range and more importantly the operating temperature of QCLs [60]. We further discuss QCLs in section 2.4.

2.2 Photoconduction and optical rectification

Photoconduction and optical rectification are the workhorse methods for producing broadband pulsed THz waves for use in time-domain spectroscopy experiments. In the former, a photoconductive antenna is fabricated by assembling two metal electodes, biased with a constant voltage, on a high-speed photoconductor substrate such as high-resistivity GaAs. Ultrafast near-infrared pulses, with frequency larger than the bandgap of the material are directed towards the space between the electrodes, creating electron-hole pairs in the photoconductor. These in turn accelerate due to the bias voltage, thus constituting a transient photocurrent which varies in time depending on the intensity envelope of the incident laser pulse and in the process radiates single-cycle THz pulses. The process is illustrated schematically in figure 2.1. The intensity and bandwidth are affected by various parameters like the characteristics of the excitation pulse, the geometric parameters of the antenna, the size of the applied voltage and material properties. The latter in turn includes the effective electron mass, the maximum electron drift velocity and the breakdown field, which determines the maximum voltage than can be applied between the electrodes [33]. This technique has allowed output powers at least as high as

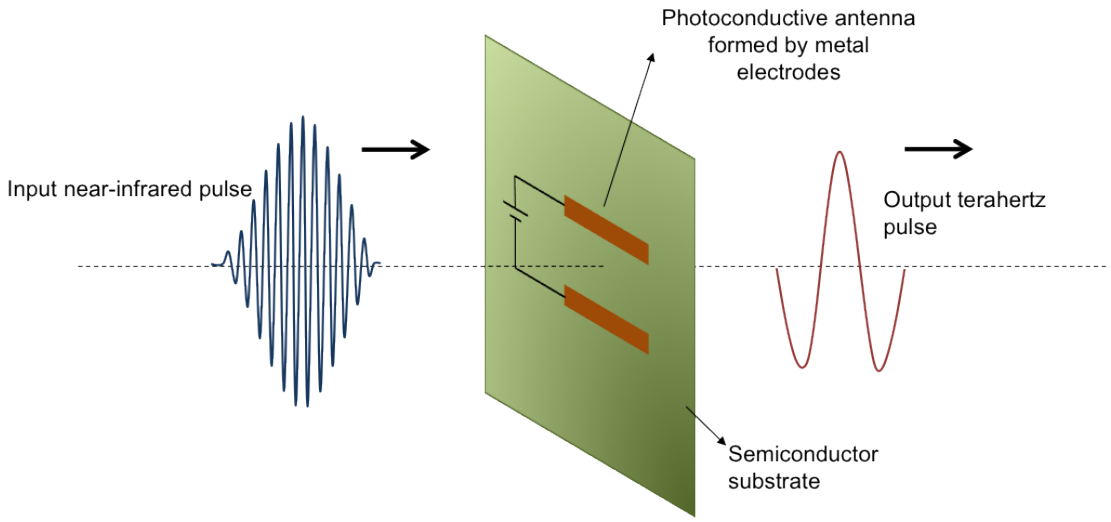


Figure 2.1: Schematic for terahertz single cycle pulse generation by photoconductance. A near infrared pulse incident on a photoconductive antenna induces a time varying photocurrent causing emission of radiation in the terahertz range.

40 μW [52] and bandwidths of 4 THz [53]. More recently, ultrabroadband pulses of bandwidths in excess of 20 THz have been observed [54], well within the ranges needed for THz time-domain spectroscopy.

The alternative mechanism for producing THz pulses, optical rectification is a non-linear process based on the inverse process of the electro-optic effect [55]. In a non-linear crystal, a dc polarization can be generated by an intense enough optical beam. Because of the second order dependence of the polarization on the applied electric field, the polarization need not reverse exactly when the field is reversed leading to a net polarization for an applied field which varies sinusoidally. This dc polarization does not radiate. However, when the incident light is a broadband pulse, this polarization is time dependent and electromagnetic waves can therefore be emitted. The incident electromagnetic pulse can be Fourier decomposed into its various frequency components. The non-linear interaction between any two frequency components will induce a polarization that oscillates at the beat frequency of the two components. Thus the component of the polarization that oscillates at

a frequency Ω can be written as [56]

$$P_i(\Omega) = \int_{\nu_0-\Delta\nu/2}^{\nu_0+\Delta\nu/2} \chi_{ijk}(\Omega,\nu) E_j(\nu+\Omega) E_k^*(\nu) \mathrm{d}\nu, \tag{2.1}$$

where ν_0 is the central frequency of the incident pulse and $\Delta\nu$ is the bandwidth. χ_{ijk} is element of the non-linear susceptibility tensor for the crystal and $E_j(\nu)$ is the Fourier transform of the j^{th} component of the electric field of the incident pulse. In the dipole far-field approximation, a particular frequency component of the output electromagnetic radiation $E_{output}(\Omega)$ is proportional to the induced polarization $E_{output}(\Omega) \propto \Omega^2 P(\Omega)$. The output radiation contains frequency components ranging from dc to $\Delta\nu$ and by an appropriate choice of the incident pulse, the output radiation can be made to be a THz pulse. Because the generally low coupling efficiencies of the incident beam to the THz output due to typically lower second order susceptibilites, the optical rectification requires high excitation pulse intensities and usually provides lower powers than photoconductive antennas but can produce pulses of higher bandwidths, of up to 50 THz [61].

2.3 Free Electron Lasers

In a free electron laser (FEL), electromagnetic radiation is generated by extracting the kinetic energy of relativistically moving electrons. A beam of fast moving electrons is transversely excited as it is directed through the spatially periodic transverse magnetic field produced by a device called an undulator (or a wiggler). The charge carriers undulate and hence emit photons as a result of being accelerated by the magnetic fields. A schematic of the process is shown in figure 2.2.

The undulator produces a magnetic field in the vertical y-direction with a sinusoidal variation along the direction of propagation of the electron beam, the z-direction, following $B_y = B_0 \sin(k_u z)$, where $k_u = 2\pi/\lambda_u$ with λ_u being the un-

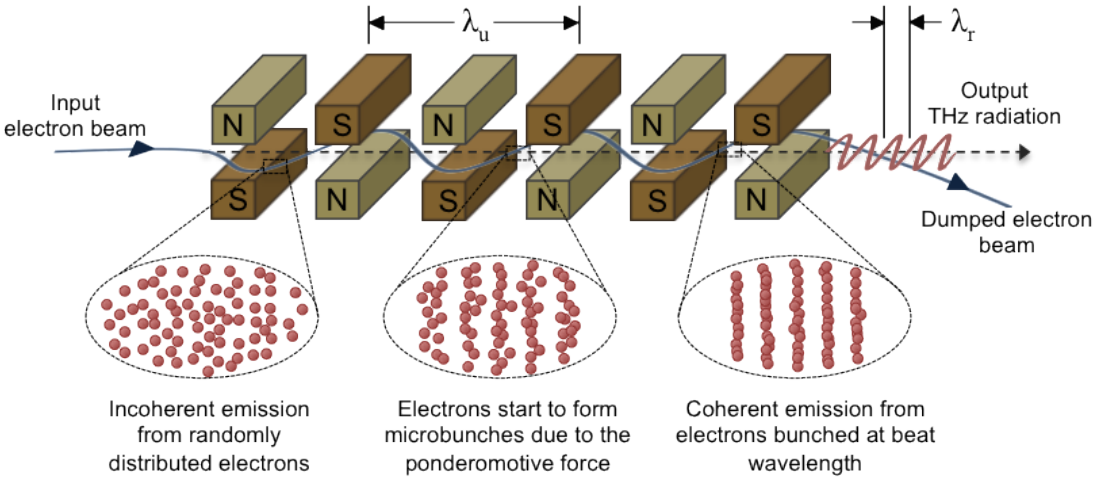


Figure 2.2: Schematic of a free electron laser. An electron beam is directed through an undulator with a spatially periodic magnetic field of period λ_u. The latter, through the transverse acceleration it induces in the moving electron mediates the interaction between the electrons beam and the output radiation which is emitted at the resonant wavelength λ_r.

dulator period. The output radiation, initially emitted via spontaneous emission co-propagates with the electrons. Only radiation of wavelength that allows for the phase of the electron's transverse oscillatory motion to be in synchrony with the phase of the E-field of the radiation it experiences can be resonantly emitted. The co-propagating radiation wavefront always moves ahead of the electron and only those that lead the electron by one wavelength after one undulator period are resonant. If the average drift speed of the electron along the z-direction is v_z, the time to travel one undulator period is $t = \lambda_u/v_z$. In that same time, the wavefront needs to travel a distance $\lambda_u + \lambda_r$, λ_r being the resonant wavelength. Therefore $t = (\lambda_u + \lambda_r/c)$ which gives the expression for the output radiation as

$$\lambda_r = \lambda_u \frac{1 - v_z/c}{v_z/c}. \tag{2.2}$$

Taking relativistic effects into account this can be written as [62]

$$\lambda_r = \frac{\lambda_u}{2\gamma_0^2}\left(1 + \frac{K_0^2}{2}\right), \tag{2.3}$$

where γ_0 is the electron energy in terms of the rest energy mc^2 and K_0 is the undulator parameter defined as

$$K_0 = \frac{eB_0}{mck_u}. \tag{2.4}$$

The resonantly emitted wavelength can therefore be tuned either by varying the kinetic energy of the electrons or the parameters of the undulator. The radiation emitted by the electrons right after entry into the undulator, although monochromatic is incoherent because the electrons, being randomly and on average uniformly distributed within the beam, the phases of their contributions to the output radiation are uncorrelated. However as the electrons propagate through the undulator a positive feedback process causes the electrons to form evenly separated microbunches resulting in coherent output radiation. Consider electrons travelling along a beam together with a co-propagating electromagnetic plane wave at the resonant output wavelength. The transverse oscillatory motion of the electron is dictated by the undulator. Hence the phase of the transverse electron motion depends on its axial position within the undulator. Depending on the phase difference between the transverse electron motion and the electromagnetic wave some electrons lose energy to the output field and are slowed down while others gain energy and are accelerated via an axial ponderomotive force, the origin of which is the interaction between the transverse magnetic field of the output radiation and the transverse electron motion. The resulting effect is that the faster electrons catch up with the slower ones forming bunches around positions for which propagating electrons lose energy to the output field. The contributions to the output radiation from the electrons therefore start to interfere constructively, thus building

up the electromagnetic field which in turn enhances the microbunching effect until saturation is reached. The beam experiences an exponential growth in intensity with distance travelled through the undulator. This process is illustrated in figure 2.2. The wavenumber of the microbunch pattern is the sum of the undulator and output radiation wavenumbers.

The amplification process described above can originate from the shot noise due to spontaneous emission of electrons in which case the FEL is said to be in a self-amplified spontaneous emission (SASE) amplifier configuration. Alternatively, the FEL can operate as a master oscillator power amplifier (MOPA) whereby the emitted radiation grows from a seed signal injected into the FEL. At output wavelengths for which good mirrors exist and for cases where the FEL is operating in a low gain regime where the radiation is amplified only by a modest amount after one pass through the undulator, the latter can be confined within a cavity. This is the case for many FELs operating in the terahertz regime and allows the wave to grow after multiple passes [62, 63]. A fraction of the radiation inside the cavity is then coupled for output with the loss of radiation in the cavity being balanced by stimulated emission from electrons thus enabling stable operation.

As mentioned above, free electron lasers are large-scale facilities and while it is obvious they are not viable as a source of THz radiation for practical applications involving the cooling scheme presented in this thesis, their umatched output power and frequency range makes them an indispensable tool for characterising material samples for potential candiates of the cooling scheme as they allow the non-linear effects to be studied.

2.4 Quantum Cascade Lasers

Quantum cascade lasers (QCLs) are a type of semiconductor laser. However, unlike conventional semicondutor lasers where the lasing medium is a bulk semiconductor and the laser transition consists of electron-hole pair recombination between the valence and conduction bands, laser operation in QCLs is achieved by intersubband transitions. The lasing medium consists of a superlattice composed of a series of thin alternating layers of materials with different band gaps. Usually layers of a lower band gap semiconductor such as GaAs are sandwiched between layers of the higher band gap AlGaAs forming a series of quantum wells, termed a quantum well heterostructure. An external electric field applied across the material produces a staircase potential profile for the electrons, as shown in figure 2.3. This leads to a splitting of the energy band into subbands where a particular subband describes the energy dispersion of electrons confined in a particular quantum well. An intersubband transition thus consists of an electron tunneling from one quantum well to the next, into a lower energy state. Such transitions can be radiative processes, and it is possible, by adequate engineering of the layer thicknesses and the applied field, to sustain a population inversion between the higher and lower energy states. An example of a lasing transition could be a hopping from the first excited state of a given quantum well to the ground state of the next well in which case the lasing frequency ω_L can be written

$$\hbar\omega_L = \epsilon_1 - \epsilon_0 + eEa, \tag{2.5}$$

where ϵ_1 and ϵ_0 are respectively the bare first excited and ground state energies of the quantum wells, E is the external applied field and a is the average distance separating the wells. The lasing frequency can thus be tuned by varying the applied electric field.

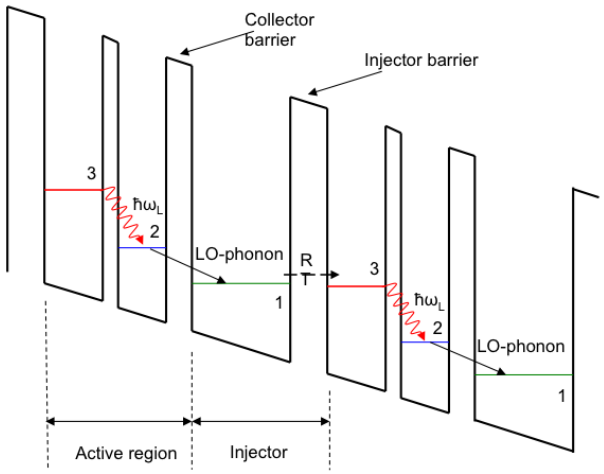


Figure 2.3: Potential profile of a QCL heterostructure employing a 3-well resonant phonon design. Lasing occurs at the frequency ω_L between the levels 3 and 2. The lower laser level is rapidly depopulated to level 1 in the injector via LO-phonon emission. Electrons are then fed to the upper laser level in the next repeat unit via resonant tunelling (RT).

While several varying designs of these heterostructures exist today [65], they all exhibit some salient and common features. The heterostructures all exhibit a repeating structure consisting of a large number (typically around a hundred) of repeating units. Each repeat unit consists of an active region and an injector. The active region is where the laser transition occurs. After an electron undergoes a transition to the lower energy level, the injector couples it to the higher energy level in the active region of the adjacent repeat unit. The electron can thus decay again to the lower level and hops to the subsequent unit, 'cascading' down energy levels as it does so. They are then extracted at one end of the superlattice and fed back to the other end.

To maintain population inversion, several design features have to be considered. We here look at those of a resonant-phonon type superlattice, one of the most simple yet most successful for high temperature operation [66]. Firstly, while it is desirable to have a small enough decay lifetime τ_{32} between the upper laser level (level 3 in figure 2.3) and the lower level (level 2) so as to obtain significant gain, it is also

important that it be not so small as to impede the sustenance of a population inversion. Therefore the layer thicknesses are usually tailored to limit the overlap of the wavefunctions of the upper and lower level states thus reducing τ_{32} and also to restrict decay from the upper level by other non-radiative processes such as via the longitudinal-optical (LO) phonon. Fast depopulation of the lower laser level followed by fast repopulation of the upper laser level in the subsequent repeat unit is also crucial. The former is achieved by engineering the energy level (level 1 in figure 2.3) in the injector part of the repeat unit such that electrons can quickly scatter into the injector by emitting an LO-phonon. For fast repopulation, the quantum wells are designed such that, when the external electric field is applied, the energy of level 1 in the injector matches the upper laser level 3 of the next repeat unit. Electrons can therefore resonantly tunnel to the upper laser level. In a typical device, the latter would have a lifetime of a few picoseconds while those of levels 2 and 1 would be of the order of tenths of picoseconds. Other types of active region and injector exist like the chirped superattice, bound-to-continuum and interlaced designs employing different methods for producing population inversion [65].

The biggest limitation of THz QCLs is their low operating temperature. However, after a decade of development, this has vastly improved from 50 K [59] to 199.5 K [66]. They are in fact currently the brightest continuous wave (c.w) solid state sources operating above liquid nitrogen temperatures [65]. While they do not currently operate at room temperature, a feature highly desirable for practical and commercial applications, their present temperature requirement sits well within reasonable ranges for laboratory research purposes. It is also worth mentioning that room temperature THz sources based on infrared QCLs have been demonstrated [67] indicating high prospects for a room temperature compact THz source in the near future. Output powers of up to 130 mW in c.w operation and peak pulsed powers exceeding 1 W [68, 69] and spectral coverage of 0.84 - 5.0 THz [65]

along with its degree of frequency tunability make the THz QCL a very eligible candidate for implementing the laser cooling scheme presented in this thesis.

We have explored in this chapter various lines of research towards developing terahertz sources and singled out those most relevant for experimentally implementing the scheme proposed in this thesis. While further advancements are required before commercial devices can be realised it is expected that the current capabilities of THz technology should enable laboratory demonstrations of the cooling principle.

Chapter 3

Laser cooling in atomic systems

In 1970 Ashkin hypothesised that the acceleration experienced by atoms and molecules from the saturated value of the radiation pressure produced by visible laser light would be significant enough to allow them to be deflected in circular orbits or trapped [70, 71]. This was indeed demonstrated two years later [72]. The idea was taken further when it was later realised, first in 1975 by Hansch *et al.* [73] treating atoms and later independently by Wineland *et al.* treating ions [74] that radiation pressure could be used to cool a low density gas. By illuminating a gas of atoms or ions isotropically with quasi-monochromatic light restricted to the lower-frequency half of the Doppler width of a resonance, particles would have a larger scattering cross-section for a counter-propagating laser beam than a co-propagating one, resulting in an average damping force exerted on the atoms, thus decreasing their average kinetic energy. This technique became known as Doppler cooling and is the main subject of discussion in this chapter.

The first demonstration of cooling occured three years later when bound magnesium ions in a Penning trap [75] were cooled to below 40 K. A further milestone was reached in 1982 by Phillips *et al.* when Askhin's proposal was applied to slow a beam of sodium atoms using an apparatus setup called a Zeeman slower [76].

It was not until 1985 that Doppler cooling free atoms from thermal temperatures was achieved in the laboratory when Chu *et al.* managed to bring sodium atoms down to $\approx 240\,\mu\mathrm{K}$ [77]. During the decades that followed, laser cooling techniques were improved and new cooling mechanisms were discovered [78,79,81] and demonstrated [80, 82–84] allowing temperatures as low as 100 nK to be reached [82]. An extensive review of the developments in this field is beyond the scope of this thesis and can instead be found in [85–87]. We will here focus on aspects pertinent to our research.

The aim of this chapter is to describe the salient theoretical elements involved in the laser cooling of free atoms, which we intend to import in developing a cooling scheme for layered superconductors. Particular attention is paid to Doppler cooling as this is the technique our scheme is largely inspired from. We thus begin with a discussion of atom-light interaction, treating the two-level atom which will provide the necessary foundation for a theoretical description of Doppler cooling presented next. The chapter ends with brief outlines of other so called sub-Doppler cooling mechanisms intended to give a broader insight into the topic and which could constitute potential resources for furthering the research presented here.

3.1 Atom-light interaction

When an atom in its electronic ground state is irradiated with monochromatic laser light of frequency resonant with the energy difference between the ground state and a particular excited state, a photon can be absorbed, inducing a transition to the excited state. Within a timescale corresponding to the lifetime of the upper level, the electron decays back to the ground state via spontaneous emission where it can subsequently be re-excited and the process continues as long as the external light field is present. An important parameter required for a quantitative semiclassical

treatment of Doppler cooling is the rate R at which photons are scattered by the atom given the incident radiation has intensity I and frequency ω, where we define a scattering event as a photon absorption followed by spontaneous emission. Since we intend to proceed by close analogy with atomic systems when treating the case of layered superconductors in Chapter 5, it is worth describing the origin of this quantity here.

For sufficiently narrowband radiation, whereby the atom is excited to only one particular excited state and where spontaneous decay always takes the atom back to the ground state, it is sufficient to consider the atom as possessing only two energy levels, a system called the two-level atom [88]. In the dipole approximation, where we consider the electric field of the applied radiation to be uniform over the spatial extent of the atom, the Hamiltonian for the system may be written as [89]

$$H = H_0 + H_I(t), \tag{3.1}$$

where H_0 is the unperturbed atomic Hamiltonian in the absence of any externally applied electromagnetic field. It has for eigenstates the ground state and excited state of the two-level atom with eigenvalues E_1 and E_2 respectively. Writing the ground state $|1\rangle$ and excited state $|2\rangle$ of the two-level atom as

$$|1\rangle = \begin{pmatrix} 1 \\ 0 \end{pmatrix}, \tag{3.2a}$$

$$|2\rangle = \begin{pmatrix} 0 \\ 1 \end{pmatrix}. \tag{3.2b}$$

H_0 can be written in the basis of these two states as

$$H_0 = \begin{pmatrix} E_1 & 0 \\ 0 & E_2 \end{pmatrix}. \tag{3.3}$$

$H_I(t) = -\hat{\mu}.\mathbf{E}\cos\omega t$ describes the electric dipole interaction between the atom and the field. $\hat{\mu}$ is the electric dipole moment operator of the atom given by $-e\hat{\mathbf{r}}$, $\hat{\mathbf{r}}$ being the operator for the position of the electron with respect to the centre of mass of the atom. For a two-level atom the ground and excited states form a complete set of eigenstates. A general quantum state of the atom can therefore be written as a superposition of these as

$$|\psi(t)\rangle = c_1(t)\, e^{-iE_1 t/\hbar}\, |1\rangle + c_2(t)\, e^{-iE_2 t/\hbar}\, |2\rangle, \tag{3.4}$$

where E_1 and E_2 are the energies of the ground and excited state respectively. Our aim is to solve for the amplitudes $c_1(t)$ and $c_2(t)$ which contain information about the time evolution of the population levels in the upper and lower energy quantum states. Substituting the expression for $|\psi(t)\rangle$ into the time-dependent Schrödinger equation

$$i\hbar \frac{\partial|\psi(t)\rangle}{\partial t} = H\,|\psi(t)\rangle, \tag{3.5}$$

we obtain the equations

$$i\dot{c_1} = \Omega\, \cos(\omega t)\, e^{-i\omega_0 t}\, c_2, \tag{3.6a}$$

$$i\dot{c_2} = \Omega^*\, \cos(\omega t)\, e^{i\omega_0 t}\, c_1, \tag{3.6b}$$

describing the time evolution of $c_1(t)$ and $c_2(t)$ where $\omega_o = E_2 - E_1/\hbar$ and Ω is called the Rabi frequency. It is given by $\Omega = \langle 1|e\hat{\mathbf{r}}.\mathbf{E}|2\rangle/\hbar$. Since $\hat{\mathbf{r}}.\mathbf{E}$ is an odd parity operator, the terms in $\langle 1|e\hat{\mathbf{r}}.\mathbf{E}|1\rangle$ and $\langle 2|e\hat{\mathbf{r}}.\mathbf{E}|2\rangle$ vanish. Expanding $\cos(\omega t)$

as $\frac{1}{2}\{e^{i\omega t} + e^{-i\omega t}\}$ in equations 3.6 we arrive at

$$i\dot{c_1} = \frac{\Omega}{2}\left\{e^{-i(\omega+\omega_0)t} + e^{i(\omega-\omega_0)t}\right\} c_2, \tag{3.7a}$$

$$i\dot{c_2} = \frac{\Omega}{2}\left\{e^{i(\omega+\omega_0)t} + e^{-i(\omega-\omega_0)t}\right\} c_1, \tag{3.7b}$$

where we have assumed Ω to be real. For small detunings δ where $\delta = (\omega - \omega_0)$ the terms in $(\omega+\omega_0)$ are much faster oscillating and over any reasonable interaction time, they average to zero. They can thus be discarded. The above step, called the Rotating Wave approximation can be further justified by noting that upon integration with respect to time, they will bear denominators having terms in $(\omega+\omega_0)$ making them much smaller than terms in $(\omega-\omega_0)$. The coupled equations 3.7 then reduce to

$$i\dot{c_1} = \frac{\Omega}{2}\, e^{i\delta t}\, c_2, \tag{3.8a}$$

$$i\dot{c_2} = \frac{\Omega}{2}\, e^{i\delta t}\, c_1, \tag{3.8b}$$

and can be solved to obtain for $|c_2(t)|^2$, the population of the upper level the expression

$$|c_2(t)|^2 = \frac{\Omega^2}{\Omega^2 + \delta^2}\, \sin^2\left(\frac{\sqrt{\Omega^2 + \delta^2}}{2} t\right). \tag{3.9}$$

The above equation describes the so called Rabi oscillations between the upper and lower levels. This coherent evolution is valid only for short timescales, smaller that the lifetime τ_{spon} against spontaneous decay which we have so far not accounted for. To do so, we first consider the expectation value of the electric dipole moment of the atom. For a general state of the two level system given by equation 3.4, the expectation of the electric dipole moment along a particular axis can be written as

$$\begin{aligned}\mu_i &= -\langle\psi(t)|\, e\hat{x}_i\, |\psi(t)\rangle \\ &= -e\left\{c_2^* c_1\, X_{21}\, e^{i\omega_0 t} \,+\, c_1^* c_2\, X_{12}\, e^{-i\omega_0 t}\right\}, \end{aligned} \tag{3.10}$$

where $X_{21} = X_{12}^* = \langle 2|\, \hat{x}_i\, |1\rangle$. Now, the density matrix for the atomic state in this basis is

$$|\psi\rangle\langle\psi| = \begin{pmatrix} |c_1|^2 & c_1 c_2^* \\ c_2 c_1^* & |c_2|^2 \end{pmatrix} = \begin{pmatrix} \rho_{11} & \rho_{12} \\ \rho_{21} & \rho_{22} \end{pmatrix}. \tag{3.11}$$

Recognising $c_2^* c_1$ and $c_1^* c_2$ as the off diagonal elements (called the coherences) ρ_{12} and ρ_{21} of the density matrix and defining $\tilde{\rho}_{12} = \rho_{12} e^{-i\delta t}$ and $\tilde{\rho}_{21} = \rho_{21} e^{i\delta t}$, the electric dipole moment can be recast as

$$\mu_i = -eX_{12}(u\cos\omega t + v\sin\omega t), \tag{3.12}$$

where we have assumed X_{12} is real. u and v are given by

$$u = \tilde{\rho}_{12} + \tilde{\rho}_{21}, \tag{3.13a}$$

$$v = -i(\tilde{\rho}_{12} - \tilde{\rho}_{21}). \tag{3.13b}$$

They can be interpreted as the in phase and quadrature components of the electric dipole with respect to the applied field respectively. Their evolution in time together with those of the diagonal terms (populations) of the density matrix can be worked out from equations 3.8 giving

$$\dot{u} = \delta v, \tag{3.14a}$$

$$\dot{v} = -\delta u + \Omega w, \tag{3.14b}$$

$$\dot{w} = -\Omega v. \tag{3.14c}$$

The term w is called the population difference and is given by $w = \rho_{11} - \rho_{22} = 1 - 2\rho_{22}$. So far, we have merely re-written equations 3.8 in terms of the u, v and w. Besides being a very useful way of visualising the evolution of the quantum state of an atom subject to monochromatic radiation[1], the form of the above equations allow us to present a phenomenological treatment of spontaneous emission below.

Since $\dot{w} = -2\dot{\rho}_{22}$ equation 3.14c gives

$$\dot{\rho}_{22} = \frac{\Omega}{2} v. \tag{3.15}$$

In Einstein's treatment of the interaction of atoms with radiation [91], spontaneous emission is modelled by a damping term in the rate equation describing population N_2 in the upper level. Given an ensemble of N atoms, N_2 is simply given by $N_2 = \rho_{22} N$. We can therefore account for spontaneous emission in equation 3.15 by adding a similar damping term thus giving

$$\dot{\rho}_{22} = \frac{\Omega}{2} v - \Gamma \rho_{22}, \tag{3.16}$$

where Γ is the spontaneous decay rate (equal to the Einstein A coefficient [91]) also known as the longitudinal decay rate [92]. The population ρ_{22} depends on $c_2^* c_2$

[1]The quantities u, v and w are in fact the components of a 3-dimensional vector called the Bloch vector. For a quantum system described by a two-dimensional Hilbert space, any general state of the system can be mapped onto a particular point on the surface of a sphere of unit radius. This representation, called the Bloch representation allows the visualisation of a quantum state as a 3-dimensional Bloch vector and time evolution of the quantum state is represented as rotations of the Bloch vector [90].

(they are equal for a pure state). Since the coherences and hence the terms u and v contain the quantum amplitude c_2 we expect them to similarly undergo exponential decay as a result of spontaneous emissions. This is therefore accounted for by adding damping terms $-\gamma_\perp u$ and $-\gamma_\perp v$ to equations 3.14a and 3.14b respecively. $\gamma_\perp$ is traditionally called the transverse decay rate [92]. It turns out that in the absence of purely dephasing processes that lead to a further loss of coherence such as atomic collisions, $\gamma_\perp$ is related to Γ by [92]

$$\gamma_\perp = \frac{\Gamma}{2}. \tag{3.17}$$

Although the above result in principle requires a quantum mechanical treatment of spontaneous emission [93] it can be justified by an argument similar to one presented in [94] by modeling an atom undergoing spontaneous decay as a damped classical oscillating dipole. The dipole moment is defined as $\vec{p} = e\vec{x}$, where e is the electron charge and $\vec{x}$ is the position of the electron with respect to the atomic nucleus. In our model, the magnitude of the dipole moment as a function of time $p(t)$ can be written as

$$p(t) = p_0 e^{-\gamma_p t} \cos \omega_0 t. \tag{3.18}$$

Comparing the above expression with equation 3.10 for the expectation value of the dipole moment and noting that in the absence of an applied field, the coherences would simply decay as $e^{-\gamma_\perp t}$ we can make the connection $\gamma_p = \gamma_\perp$. In the far field limit, the electric field produced by the oscillating dipole is proportional to $\dot{p}(t)$ and its size may be written as

$$E(t) = E_0 e^{-\gamma_\perp t} \sin \omega_0 t. \tag{3.19}$$

The average power $\bar{P}$ radiated is proportional to E^2 and can thus be written as

$$\bar{P}(t) \propto E_0^2 e^{-2\gamma_\perp t}. \tag{3.20}$$

Moving to a quantum picture, the power emitted is equal to $\hbar\omega_0$ times the rate of photons emitted which is equal to the rate of decay from the upper energy level and therefore from equation 3.16 in the absence of an applied field varies as $\dot{\rho}_{22} \propto e^{-\Gamma t}$. Comparing this with the above equation, we can therefore make the connection $\gamma_\perp = \Gamma/2$.

We thus finally obtain

$$\dot{u} = \delta v - \frac{\Gamma}{2}u, \tag{3.21a}$$

$$\dot{v} = -\delta u + \Omega w - \frac{\Gamma}{2}v, \tag{3.21b}$$

$$\dot{w} = -\Omega v - \Gamma(w - 1). \tag{3.21c}$$

These are called the Optical Bloch equations [90] describing the interaction of a two level atom with near resonant radiation in the presence of spontaneous decay. For long interaction times ($t \gg \Gamma^{-1}$), when the steady state is reached, setting $\dot{u} = \dot{v} = \dot{w} = 0$, we obtain the population of the upper level as

$$\rho_{22} = \frac{\Omega^2/4}{\delta^2 + \Omega^2/2 + \Gamma^2/4}. \tag{3.22}$$

At this point, the rate of spontaneous decay and hence the scattering rate is given by $R_{scatt} = \Gamma\rho_{22}$.

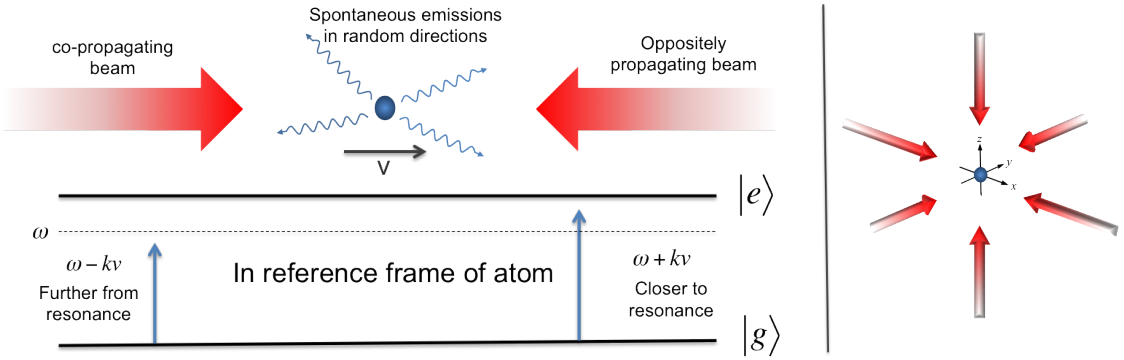
3.2 Doppler cooling

Conservation of momentum requires that when an atom undergoes an electronic transition induced by the absorption of a photon, it experiences a recoil equal to the momentum of the photon absorbed. Since in the subsequent spontaneous decay a photon is emitted in a random direction, on average the momentum imparted to an atom in one scattering process is $\hbar k$ with k being the photon wavenumber. The average scattering force acting on an atom may therefore be written as

$$\begin{aligned} \bar{F}_{scatt} &= \hbar k \, R_{scatt} \\ &= \hbar k \Gamma \frac{\Omega^2/4}{\delta^2 + \Omega^2/2 + \Gamma^2/4}. \end{aligned} \tag{3.23}$$

As the applied laser light intensity is increased to infinity ($\Omega \to \infty$), the scattering force attains a maximum value of $\bar{F}_{max} = \hbar k \Gamma/2$. Taking a sodium atom as example, for a d-line transition, this amounts to a maximum acceleration of the atom of about $9 \times 10^5 \, \mathrm{ms}^{-2}$ [90] which is a very large figure. In principle therefore, the scattering force can have a significant effect on the motion of atoms and constitutes a potential tool for slowing down a beam of atoms. Indeed if we consider the above mentioned transition which has resonant wavelength of 589 nm and excited state lifetime of 1.6 ns, assuming a deceleration at half the maxium rate, a sodium atom initially moving at $1000 \, \mathrm{ms}^{-1}$ (Which corresponds to the most probable speed in a gas at 900 K) would be stopped within a distance of about 1.1 m [90]. This shows the experimental feasiblity of slowing atoms via the scattering force agreeing with the discussion by Ashkin [70, 71].

Additionally, it is possible to cool a gas of atoms by radiation pressure. To do so requires a setup such that the net scattering force always opposes the velocity of the atoms. Such a setup is illustrated for cooling in one dimension in figure 3.1a.



(a) Doppler cooling (b) Optical molasses

Figure 3.1: (a): Schematic setup for doppler cooling. An atom is shone with two counter-propagating beams of monochromatic laser light red detuned from the resonance. In the reference frame of an atom moving at velocity v, light from the oppositely propagating beam appears blue-shifted closer to resonance increasing the average scattering rate from that beam while light from the beam co-propagating with the atom is red-shifted further away from resonance causing a decrease in the average scattering rate from the beam. (b): Schematic of optical molasses setup with six laser beams along the 3 axes for cooling in 3 dimensions.

An atom having velocity v is irradiated by two counter-propagating laser beams of monochromatic light detuned below the resonance frequency ω_0 of an particular electronic transition. The moving atom sees light from the laser source it moves towards Doppler shifted closer to the resonance frequency, while light from the other laser is red shifted further away from resonance. From the expression in equation 3.23 for the scattering force, it can be seen that because the effective detuning for light from the beam that co-propagates with the atom is larger, the atom predominantly scatters photons from the oppositely travelling beam. The resulting imbalance in scattering forces from the two beams produces a net retarding force on the atom. The force can be expressed mathematically by considering the scattering force $F(\delta)$ as a function of the detuning $\delta = \omega - \omega_0 \pm kv$. The net average force on the atom can thus be written as

$$\bar{F}_{net} = \bar{F}_{scatt}(\omega - \omega_0 + kv) - \bar{F}_{scatt}(\omega - \omega_0 + kv), \tag{3.24}$$

where ω is the frequency of the laser, ω_0 is the resonant transition frequency for an atom at rest and the term $\pm kv$ is the low speed limit of the Doppler shift seen by the atom (negative for the co-propagating beam and positive for the oppositely travelling one). For low velocities, where the Doppler shift is much smaller than the natural linewidth of the transition ($kv \ll \Gamma$), we can Taylor expand the force around $\delta = \omega - \omega_0$ and obtain to first order in kv

$$\begin{aligned} \bar{F}_{net} &\approx \left[\bar{F}_{scatt}(\omega - \omega_0) - kv\frac{\partial \bar{F}}{\partial \omega}\right] - \left[\bar{F}_{scatt}(\omega - \omega_0) + kv\frac{\partial \bar{F}}{\partial \omega}\right] \\ &= -\alpha v, \end{aligned} \tag{3.25}$$

where

$$\alpha = 2k\frac{\partial \bar{F}}{\partial \omega} = -4\hbar k^2 \frac{2\Omega^2}{\Gamma^2} \frac{2\delta/\Gamma}{[1 + (2\delta/\Gamma)^2 + 2\Omega^2/\Gamma^2]^2}. \tag{3.26}$$

We will further restrict this treatment to the case of low laser intensities so that the Rabi frequency Ω is much smaller than the spontaneous decay rate Γ. The last term in the denominator in the above expression can therefore be dropped. This also avoids complications with saturation and allows us to treat the force from each beam as acting independently. As expected, we note that a negative value of δ (red detuning) makes α positive and hence produces a damping force which would in principle result in an exponential decay of the velocity of the atom until it comes to rest. We should not forget however that the force considered above is only the average of the scattering force which is in fact stochastic in nature. The only safe conclusion from equation 3.25 is that the average velocity $\langle v \rangle$ is brought to zero. In reality, at equilibium, the atom will have range of possible velocities given by a probability distribution $P(v)$. The relevant parameter here however, that helps quantify the effectiveness of this scheme, is the minimum achievable temperature

called the Doppler cooling limit. We are thus interested in the kinetic energy of the atom rather than the velocity. Our objective is to work out the mean squared velocity $\langle v^2 \rangle$ at the later stages of cooling from which we can deduce the minimum temperature using the equipartition relation $\frac{1}{2}M\langle v^2 \rangle = \frac{1}{2}k_{\mathrm{B}}T$, with M being the mass of the atom. We shall first decompose the stochastic scattering force F_{scatt} into a mean force $\bar{F}_{\mathrm{scatt}}$ and a random force η_{scatt} of zero mean[2] whose effect on $\langle v^2 \rangle$ we will then work out. Under the influence of only the average force we can write,

$$\frac{\mathrm{d}}{\mathrm{d}t}\left(\frac{1}{2}Mv^2\right) = Mv\frac{\mathrm{d}v}{\mathrm{d}t} = -\alpha v^2, \tag{3.27}$$

and hence

$$\frac{\mathrm{d}}{\mathrm{d}t}\left(\frac{1}{2}M\langle v^2 \rangle\right) = -\alpha\langle v^2 \rangle. \tag{3.28}$$

The stochastic term η_{scatt} can in turn be written as $\eta_{\mathrm{scatt}} = \eta_{\mathrm{spon}} + \eta_{\mathrm{abs}}$. The randomness of the scattering force is in part due to spontaneous emission while the other contribution originates from the fact that absorption is also a random process since the atom does not always absorb the same number of photons in every unit time interval. In the following, we will account for the stochastic term by considering the effect it has on $\langle v^2 \rangle$ when acting alone starting with an atom at rest ($\langle v^2 \rangle = 0$). Since on the average random force is zero, $\langle v \rangle = 0$ at all times and hence $\langle v^2 \rangle$ is equal to the variance σ^2. The net effect of η_{scatt} is then the cumulative effects of η_{spon} and η_{abs}. Looking first at one spontaneous emission event, in 3-dimensions, the component of momentum imparted along a particular direction, say the z-direction may be written as $\hbar k \cos\theta$ with θ being the usual

[2]The force then takes the same form as the Langevin force occuring in Brownian motion which allows a similar treatment to be used here to obtain $\langle v^2 \rangle$.

polar angle in spherical coordinates. The recoil on the atom along that particular axis is $v_{\mathrm{r}} \cos\theta$ where $v_r = \hbar k/M$ is the recoil velocity. Since the photon is equally likely to be emitted in any direction, the mean square velocity component of the atom after one emission is given by

$$\langle v^2 \rangle = \int \frac{1}{4}\, v_r^2 \cos^2\theta \, \mathrm{d}\mathbf{\Omega} = \frac{1}{3}\, v_r^2. \tag{3.29}$$

For a sequence of N spontaneous emissions the total recoil on the atom is the sum of the recoils from each indvidual emission. The variance and in this case the mean squared velocity after N emissions is simply $\frac{1}{3}\, N v_r^2$. In a time t, the average number of photons scattered is $R_{\mathrm{scatt}} t$ and therefore

$$\langle v^2 \rangle(t) = \frac{1}{3}\, v_r^2\, R_{\mathrm{scatt}} t. \tag{3.30}$$

Evidently, the average number of photons absorbed in a time t is also $R_{\mathrm{scatt}} t$. Assuming the number of photons absorbed follows a Poissonian distribution[3] the variance in the number of absorbed photons is $R_{\mathrm{scatt}} t$. Since an excess or defect by one in the number of absorbed photons produces an increase in v^2 of v_r^2, we have

$$\langle v^2 \rangle_{\mathrm{abs}}(t) = v_r^2\, R_{\mathrm{scatt}} t. \tag{3.31}$$

In practice atoms are cooled along all three axes. The setup in figure 3.1a can be extended to work in three dimensions by using 6 laser beams as shown in figure 3.1b and is termed 'optical molasses' [77]. In this case, the rate of spontaneous emission is instead $6R_{\mathrm{scatt}}$. In the above equation however R_{scatt} needs to be replaced by $2R_{\mathrm{scatt}}$ since fluctuations in the force due to varying absorption rates

[3]The photon statistics in resonance fluorescence is in fact sub-Poissonian. The variance of such a distribution is usually written as $\langle n \rangle(1+Q)$ where Q is known as the Mandel parameter and accounts for departures from the Poissonian distribution [96]. For low laser intensities however, Q can be neglected to a very good approximation.

along a particular axis is affected by only two of the laser beams. Again this simplification is valid only for low intensities, far from saturation effects and where we can assume absorption from the laser beams to be uncorrelated. Under the force η only, we can thus write

$$\begin{aligned}\langle v^2\rangle(t) &= \langle v^2\rangle_{\text{spon}}(t) + \langle v^2\rangle_{\text{abs}}(t) \\ &= 2v_r^2\, R_{\text{scatt}} t + 2v_r^2\, R_{\text{scatt}} t \\ &= 4v_r^2\, R_{\text{scatt}} t. \end{aligned} \tag{3.32}$$

Differentiating with respect to time then gives

$$\frac{\mathrm{d}\langle v^2\rangle}{\mathrm{d}t} = 4v_r^2\, R_{\text{scatt}}. \tag{3.33}$$

Under the total scattering force therefore, we may write

$$\frac{\mathrm{d}}{\mathrm{d}t}\left(\frac{1}{2}M\langle v^2\rangle\right) = -\alpha\langle v^2\rangle + 2Mv_r^2 R_{\text{scatt}}. \tag{3.34}$$

The equation desribes the competition between the average cooling force that tends to minimise the average kinetic energy and the random diffusive term that tends to increase it via the fluctuations described above. After long interaction times an equilibrium value of $\langle v^2\rangle$ is reached which we can find by setting the time derivative in the equation 3.34 to zero. From this we obtain the average kinetic energy as

$$\frac{1}{2}M\langle v^2\rangle = \frac{k_{\text{B}}T}{2} = \frac{2Mv_r^2 R_{\text{scatt}}}{\alpha} = \frac{\hbar\Gamma}{4}\frac{1+(2\delta/\Gamma)^2}{-2\delta/\Gamma}. \tag{3.35}$$

The expression is minimised when $\delta = -\Gamma/2$, therefore giving a Doppler cooling limit temperature of

$$T_{\min} = \frac{\hbar\Gamma}{2k_{\mathrm{B}}}. \tag{3.36}$$

Taking the same example as above of a sodium atom d-line transition this expression implies a minimum achievable temperature $\sim 240\,\mu\mathrm{K}$. It should be pointed out that we have assumed the atomic system to be thermally isolated and as such have totally neglected any reheating of the system which would typically occur if it were in contact with a finite temperature bath. This can be accounted for by adding an additional term Q_r in equation 3.34 representing a reheating rate. In Chapter 5, we intend to develop a similar scheme to cool fluctuations in the phase of the superconducting order parameter.

While the treatment of Doppler cooling presented in this section is clearly heuristic, it presents the advantage of providing a clear physical and intuitive picture of the processes involved especially with regards to the provenance of the force fluctuations, without a large sacrifice in accuracy. Indeed the Doppler cooling limit calculated is in good agreement with the values obtained via more sophisticated methods [97–99]. Besides the assumptions already mentioned that greatly simplfy our treatment, like taking the limit of low applied laser intensity, the success of the above treatment is owing to the parameter regimes offered by atomic systems. Scattering is a quantum mechanical process and due to recoil, momentum of the atom in fact changes in discrete steps. We have however treated the motion of the atom entirely classically with only the internal electron dynamics treated quantum mechanically and assumed the latter to always be in the steady state (ρ_{22} constant). This is possible because for atoms, the recoil velocity v_r is small compared to the velocity range for which for which the resonant condition is satisfied[4] [97]. A large number of scattering events are thus required to effect any significant change in

[4]This is the velocity range that produces a corresponding Doppler broadening equal to the natural linewidth Γ.

the velocity of the atoms enough to upset the resonance condition thus allowing us to describe the exchange of momentum between the atom and the light field as a continuous process via an average scattering force. One usually speaks about the external timescales (in this case the characteristic decay time of the kinetic energy of the atom $2\alpha/M$) being much longer than internal timescales (Γ) [97,100]. Additionally, this classical treatment of the motion of the atoms is possible only when the de Broglie wavelength of the atom, which determines the spatial extent of the wavefunction of the atom's centre of mass, is small compared to the average separation of the atoms in the gas. We thus need to consider whether these conditions are satisfied when treating a different kind of system like layered superconductors.

3.3 Sub-Doppler cooling

With the advent of more accurate temperature measurement techniques, an optical molasses experiment carried out in 1988 revealed a surprising result. The temperature of a gas of sodium atoms was found to be as low as $43\,\mu\mathrm{K}$, an order of magnitude lower than the expected Doppler cooling limit [101]. It clearly indicated that other cooling mechanisms were at play. Following further theoretical investigations new cooling mechanisms based on polarisation gradients now also known as Sisyphus cooling were proposed [78, 79]. A more detailed treatment of the interaction of an atom with the standing wave pattern produced by two counter-propagating laser beams in an optical molasses setup reveals another contribution in addition to the scattering force known as the dipole force. This force can be understood classically by considering the interaction energy of an applied field with the electric dipole moment it induces in an atom. In a field of spatially varying amplitude as is the case with a standing wave[5], atoms are thus drawn to

[5]It can be understood in quantum mechanically in terms of the a.c Stark shift, also called the light shift [90]

positions of lower potential energy. The scheme also relies on the fact that atoms are not in fact two level systems. In particular, the ground state for the transition is doubly degenerate and the applied field lifts this degeneracy in such a way that positions of maximum potential energy along the standing wave for one of the degenerate levels are positions of lower potential energy for the other level and vice-versa. An atom moving along this standing wave pattern constantly exchanges kinetic and potential energy. By proper detuning of the lasers, the system can be engineered such that the atom is excited to a higher energy state when the atom is at a maximum of potential irrespective of which of the two ground states it is in. By energy conservation, an excitation from the higher energy ground state to the excited state followed by a decay to the lower energy ground state implies a net exchange of energy from the atom to the field thus decreasing the kinetic energy of the atom. This is the mechanism by which the atom is cooled and the minimum temperature achievable by this technique is given by the recoil limit [102]

$$T_{\text{recoil}} = \frac{\hbar^2 k^2}{M k_{\text{B}}}. \tag{3.37}$$

For our example of a sodium atom and considering a d-line transition, this amounts to 2.4 μK. Even this limit however has been broken by other cooling mechanisms like velocity-selective coherent population trapping [81] and Raman cooling [82] utilising velocity-selective Raman transitions. Like the Sysiphus cooling mechanism, both involve three energy levels: two lower energy levels and an excited one. This allows the atomic system to be engineered in such a way that excitation of an atom is highly sensitive to the atomic velocity so that atoms falling in a velocity range, smaller that the recoil velocity v_r centred around $v = 0$, called the dark region are then no longer excited by the laser field. The scheme works by exciting all atoms with velocities outside this range and relying on spontaneous

emission to take them into this region of velocity space after which they no longer interact with the field and are thus trapped within this region of velocity space [86].

While we have not presented a detailed description of these Sub-Doppler cooling mechanisms as they are not particularly relevant for the research presented here, the purpose of mentioning them is to point out the possible potential of going beyond the Doppler-cooling limit should corresponding conditions arise in layered superconductor systems. For example, tri-layer systems are expected to have three modes collective plasma oscillations (See Chapter 6), analogous to three atomic levels.

Chapter 4

High T_{C} Superconductors and Josephson Physics

4.1 High T_{c} Superconductors

4.1.1 Introduction and overview of superconductivity

Superconductivity, a macroscopic quantum phenomenon, is characterised by two defining features, one of which is the disappearance of all electrical resistance. This property was first discovered by H. K. Onnes [103–105]. After he had first liquefied helium in 1908 which allowed the refrigeration of samples down to a few Kelvins, Onnes began experiments where he measured the electrical resistance of metallic samples down to the temperatures achievable using the inert element as refrigerant. After a first striking observation that the resistance of a platinum wire dropped to a constant residual value below 4.25 K, Onnes suspected the resistance of higher quality samples should in fact completely vanish at these low temperatures. This was indeed observed in 1911 when the resistance of a mercury sample[1] was observed

[1]Mercury was chosen at the time as high purity samples of the metal were available and moreover, without the need for being drawn into wires - the mercury was used in a capillary - it

to drop by five orders of magnitude, to virtually zero at a critical temperature (T_c) of 4.2 K, marking the discovery of a novel state of conductivity, initially called 'supraconductivity' by Onnes but which later became known as superconductivity [107]. In the years that followed, other materials like tin and lead were found to exhibit the same transition to a superconducting state at temperatures of 4 K and 6 K respectively [106, 107].

The second defining feature of superconductivity is perfect diamagnetism: discovered in 1933 by W. Meissner and R. Ochsenfeld. In their experiments, not only did they find that a magnetic field is prevented from penetrating a superconductor[2] but also observed that tin and lead samples, initially in their normal conducting state would expel any magnetic field as the specimens were cooled below their respective critical temperatures, in contradiction to what would be expected from a perfect conductor alone [108], as is illustrated in figure 4.1. The result was incontrovertible evidence that the superconductivity Onnes had observed years before is fundamentally different from conventional perfect conduction. This prompted further investigations into the physical properties of the superconducting state, a quest for new superconductive materials, as well as research efforts in theoretical models to explain the phenomenon, still ongoing to date.

The first piece of theoretical development came from the London brothers in the form of two mathematical equations providing a phenomenological description of the microscopic electric and magnetic fields inside a superconductor [109]. These equations, which we further discuss in subsection 4.1.2 reproduce predictions of the observed phenomena of persistent currents without an external electric field and the Meissner effect.

was less prone to contamination [107].

[2]The magnetic field in fact does penetrate but only up to a usually minute distance λ known as the London penetration depth where $\lambda \sim 500$Å. Perfect diamagnetism thus applies only for bulk samples [111].

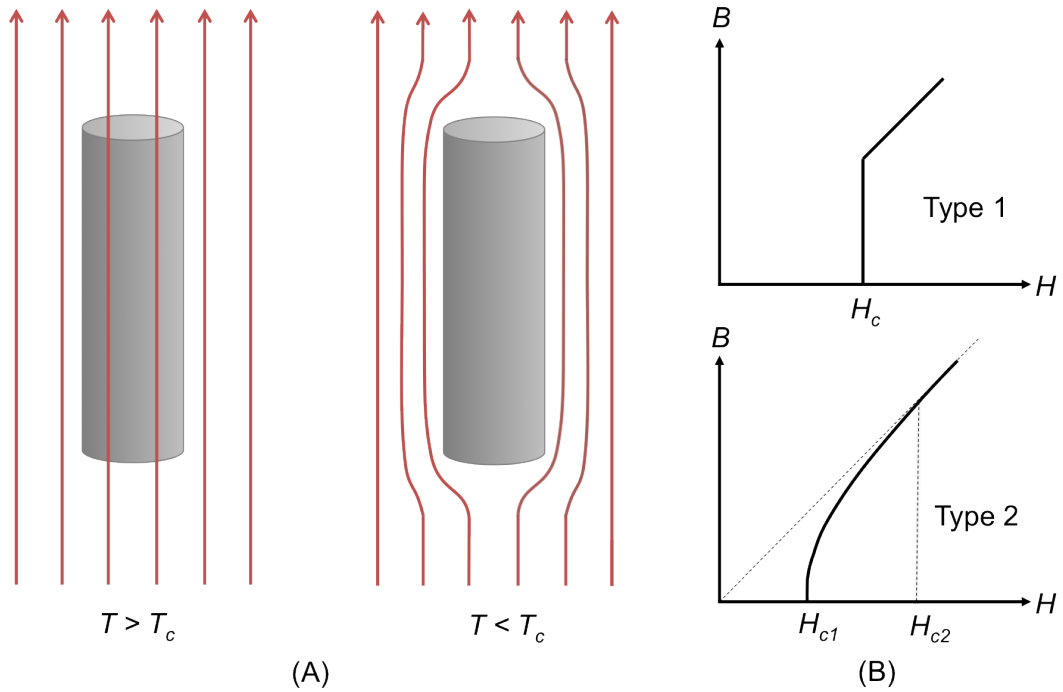


Figure 4.1: (A): Illustration of the Meissner effect. Above T_c the cylindrical sample is in the normal state and an applied magnetic field completely penetrates the specimen. This magnetic field is expelled as the material is cooled below T_c. (B): Schematic representation of the transition from superconducting to normal state as the applied magnetic field is increased. For type 1 superconductors (upper plot) there is a sudden jump in the magnetic field B inside the specimen as the critical field H_c is reached. For type 2 supeconductors (lower plot) the magnetic field starts penetrating at a lower critical field H_{c1} and the specimen is in a mixed state until an upper critical field H_{c2} is reached, where the applied field wholly penetrates the sample which transitions to the normal state.

Shielding magnetic fields out of a superconductor comes at an energy cost. It requires the build-up of screening currents that produce a field which cancels the applied field inside the sample. As such, at a certain value called the critical field H_c, it becomes more energetically favourable for the sample to revert to the normal state and therefore break superconductivity [110]. H_c is usually such that the energy per unit volume in holding the field out equals the difference in the free energy between the normal and superconducting states of the sample at zero applied field. The critical field increases from zero at the critical temperature T_c to a maximum value $H_c(0)$ at absolute zero [111]. It follows that there exists also a critical cur-

rent, the maximum current a superconducting specimen can support, given by the current for which the magnetic field at the surface of the superconductor reaches the critical field.

The transition from superconducting to normal state as the external magnetic field is increased shows two general types of behaviour. For superconductors now known as type 1, superconductivity breaks abruptly as the critical field is reached at which point the applied field wholly penetrates the sample [110] in a first-order transition [111]. An experiment carried out in 1935 on lead-thallium and lead-bismuth alloys revealed a different kind of response [112]. It was found that up to a lower critical field H_{c1}, no magnetic field penetrates the specimen while beyond a second higher critical field H_{c2} the sample loses all superconductive properties. In the range between H_{c1} and H_{c2} however, the flux partially penetrates and continuously increases until full penetration is reached at H_{c2} whilst the specimen still retains perfect conductivity, a situation called the mixed state. Materials exhibiting the latter behaviour would later become known as type 2 superconductors. The variation in B-field with applied field H for both types of superconductors are illustrated in figure 4.1.

At the time, no theoretical framework existed to explain these observations. It took a further 15 years before another phenomenological theory was devised which allowed the macroscopic treatment of superconductors in the regime where applied magnetic fields are of the order of the critical fields. The Ginzburg-Landau (GL) theory as it is called is based on Landau's theory of second-order phase transitions. A complex pseudowavefunction $\psi(\mathbf{r})$ is chosen as the order parameter, the magnitude of which, crudely speaking, measures the 'degree of superconductivity' at point $\mathbf{r}$ and vanishes at T_c [110, 111, 113]. Salient features of the theory and some important implications are outlined in subsection 4.1.3.

A further milestone in our understanding of superconductors was a series of

experimental results that all pointed towards the existence of an energy gap Δ of order $k_B T_c$ between the ground and excited electronic states of a superconducting system. One such result was the observation of an exponential dependence on temperature of the electronic specific heat of superconducting vanadium of the form $e^{-bT_c/T}$, where b is a constant, a telltale sign of such an energy gap [114, 115]. Later, Glover and Tinkham performed experiments where the frequency dependent complex conductivities of thin lead and tin films were determined from electromagnetic transmission data [116,117]. It was found that the real part of the complex conductivity was nearly zero for photon energies below roughly $3k_B T_c$ and rose rapidly up to a limiting value σ_n - the corresponding value in the normal state - as the photon energy was increased beyond $3k_B T_c$, thus further supporting the idea of an energy gap but also hinting that the electronic excitations occurred in pairs.

A breakthrough then ensued in 1957 when the first comprehensive microscopic theory of superconductivity was brought forth by J. Bardeen, L. N. Cooper and J. R. Schrieffer now widely known as the BCS theory [5]. It was built on earlier work by Cooper [118] who showed that due to their fermionic nature, two electrons, in the presence of a Fermi sphere of other electrons could form a bound pair given an attractive interaction between them, irrespective of how weak it was. In their seminal paper, Bardeen and co-authors argued that processes like electron-phonon interactions, by overcoming the repulsive screened Coulomb interaction, could produce the above conditions necessary to the formation of boson-like Cooper pairs of electrons: the superconducting charge carriers postulated in the London and GL theories. The theory supported the idea of an energy gap and provided a physical interpretation of it as the energy required to break a Cooper pair into constituent normal electrons. Among the theory's early sucesses was the ability to reproduce specific heat predictions that were in good agreement with past experiments [5].

The BCS theory is not particularly relevant to this thesis and we shall not discuss it in further detail besides noting that we will be treating the below-gap regime, where we assume that the number density of Cooper pairs is not affected by the electrodynamics of our system.

While the microscopic mechanism behind superconductivity was generally thought to be well understood with the advent and success of BCS theory, this was about to change in 1986. Theoretical research efforts in the field of superconductivity underwent a major revival following the discovery by G. Bednorz and K. A. Müller of a ceramic oxide that transitions to the superconducting state at 35 K [1]. Since this was higher than the 30 K maximum believed to be allowed by the BCS electron-phonon pairing mechanism[3] [2], it became clear that other processes were at play in this novel type of material, dubbed high temperature superconductors (HTS). This was made even more evident in later years with the discovery of other compounds belonging to the same family, the cuprates, having radically higher critical temperatures: first with the observation of T_c at 93 K in a particular variant of yttrium barium copper oxide (YBCO) a year after Bednorz [8] and later at as high as 135 K in mercury barium calcium copper oxide systems [10]. However a complete microscopic theory of the same scope as BCS theory that explains the mechanism behind high temperature superconductivity still remains elusive today [3,120]. While other classes of HTS have also been discovered like the iron-based pnictides [121] our discussion of HTS in this thesis which continues in subsection 4.1.4 will be focused on cuprates.

[3]The limit has however been adjusted following the discovery in 2001 of superconductivity at 39 K in magnesium diborate [119], which allows for an exceptionally high T_c within the BCS framework. MgB_2 currently has the highest T_c of any BCS type bulk superconductor.

4.1.2 The London Equations

In 1935 the brothers Fritz and Heinz London formulated the first theoretical model of superconductivity, relating the microscopic currents and electromagnetic fields inside a superconductor. Now known as the London equations, they provided the first quantitative description of the Meissner effect. The description, largely phenomenological, could not at the time be rigorously derived from first principles. It can nevertheless be explained by intuitive physical arguments and supported by experimental results which we outline below.

The London equations are

$$\Lambda \frac{\partial \mathbf{J_s}}{\partial t} = \mathbf{E}, \tag{4.1a}$$

$$\nabla \times \mathbf{J_s} = -\frac{1}{\Lambda}\mathbf{B}, \tag{4.1b}$$

where $\mathbf{J_s}$ is the local supercurrent density, $\mathbf{E}$ and $\mathbf{B}$ are the microscopic electric and magnetic fields respectively while $\Lambda = m/n_s e^2$. In the last expression e is the electronic charge, m is the electron mass and n_s is taken to be the number density of superconducting electrons. The first equation, referred to by the London brothers as an "acceleration equation" is intended as a replacement for Ohm's law for superconductors and serves to explain the phenomena that electric currents are sustained in a superconductor without the need for an electromagnetic field. This can be seen by setting $\mathbf{E}$ to zero in equation 4.1a. The equation can be obtained by assuming that a supercurrent is a flow of charge carried by freely moving electrons having a number density n_s. It is then simply a reformulation of the equation of motion of free electrons under the electric part of the Lorentz force,

$$m\frac{\mathrm{d}\mathbf{v_s}}{\mathrm{d}t} = -e\mathbf{E}.$$

Equation 4.1a can then be obtained by defining the supercurrent density as $\mathbf{J_s} = -en_s\mathbf{v_s}$. It is instructive to note that the above equation corresponds to the Drude model for electrical conductivity defined by

$$m\frac{\mathrm{d}\mathbf{v}}{\mathrm{d}t} = e\mathbf{E} - m\mathbf{v}/\tau,$$

taken in the limit where τ, a characteristic relaxation time, is taken to be infinite [110, 111]. The second London equation encapsulates the Meissner effect. Using Ampere's law (neglecting the displacement current[4]), $\nabla \times \mathbf{B} = \mu_0\mathbf{J}$, to substitute for the current we obtain

$$\nabla^2\mathbf{B} = \frac{\mu_0}{\lambda_L^2}\mathbf{B}, \tag{4.2}$$

where $\lambda_L = \sqrt{m/\mu_0 n_s e^2}$ is called the London penetration depth. The differential equation allows for a solution whereby a magnetic field is exponentially screened deeper within the material. Indeed, an example one-dimensional solution to a system with boundary condition $\mathbf{B}(0)$ parallel to the surface of a superconductor would be $\mathbf{B}(z) = \mathbf{B}(0)e^{-z/\lambda_L}$. We shall make use of equation 4.2 in Chapter 5 when we describe a model for the phase dynamics in layered superconductors.

4.1.3 Ginzburg-Landau Theory

In the theory developed by V. L. Ginzburg and L. Landau a complex pseudowavefunction $\psi(\mathbf{r})$ is chosen as order parameter and the formalism of Landau's theory of phase transitions is followed. Although no physical interpretation for $\psi(\mathbf{r})$ was given in their original paper, in light of the later developments brought by the BCS theory we now know that it can be thought of as the wavefunction of the centre-of-

[4]Ashcroft and Mermin [110] justify this step by assuming that "the rate of time variation is so slow that the displacement current can be neglected".

mass motion of Cooper pairs [111]. Landau's formalism posits that close enough to the critical point, where the order parameter is small, if $\psi(\mathbf{r})$ varies slowly in space, the free energy density of the system can be written as a Taylor expansion in the order parameter and its gradient $\nabla\psi$, keeping only terms that obey the symmetry of the system and satisfy other known phenomenological features of the transition. For a superconductor in an external field, an appropriate expression is

$$f = f_n + \alpha|\psi|^2 + \frac{\beta}{2}|\psi|^4 + \frac{1}{2m}\Big|\Big(-i\hbar\nabla - 2e\mathbf{A}\Big)\psi\Big|^2 + \frac{|\mathbf{B}|^2}{2\mu_0}, \tag{4.3}$$

where f_n is the free energy of the normal state in the absence of any external field, α and β are real phenomenological parameters which can be temperature dependent and $\mathbf{A}$ is the magnetic vector potential. For a general set of boundary conditions, the order parameter will adjust itself so as to minimise the total free energy of the system: the functional given by the volume integral of the free energy density f. Employing variational methods (treating the free energy density as one would a Lagrangian and invoking the Euler-Lagrange equation with respect to ψ or ψ^*) one arrives at the Ginzburg-Landau differential equation

$$\alpha\psi + \beta|\psi|^2\psi + \frac{1}{2m}\Big(-i\hbar\nabla - 2e\mathbf{A}\Big)^2\psi = 0, \tag{4.4}$$

which describes the dependence of the order parameter on the magnetic vector potential. Considering the variation with respect to $\mathbf{A}$ and applying Maxwell's equation $\nabla \times \mathbf{B} = \mu_0\mathbf{J}$ we obtain an expression for the supercurrent given by

$$\mathbf{J_s} = -\frac{ie\hbar}{2m}(\psi^*\nabla\psi - \psi\nabla\psi^*) - \frac{2e^2}{m}\mathbf{A}|\psi|^2. \tag{4.5}$$

The latter is similar to the the probability current of a charged particle in the presence of an electromagnetic field multiplied by its charge, except that here the

particle wavefunction is replaced with the order parameter also called the macroscopic wavefunction. If $|\psi(\mathbf{r})|$ is taken to be constant and equal the value that minimises the free energy in the absence of external fields, which we denote by ψ_∞, taking the curl of the above equation we obtain the second London equation 4.1b when making the correspondence $|\psi_\infty|^2 = n_s$, a regime known as the London limit. Together, equations 4.4 and 4.5 allow for a description of superconductors with more complex geometries, in the presence of high magnetic fields where the Cooper pair density $|\psi(\mathbf{r})|^2$ varies in space and is depleted in certain regions leading to the formation of superconducting and normal domains.

We have already encountered in the previous subsection a first length scale λ_L, the London penetration depth that characterises the decay length of magnetic fields inside a superconductor, also derivable from the second GL equation. The Ginzburg-Landau theory predicts another characteristic length scale ξ, known as the coherence length. To help understand its origin we consider the first GL equation in one dimension and in the absence of any field. Following Tinkham [111] we take ψ to be real and introduce a normalised wavefunction $\Psi = \psi/\psi_\infty$ where $\psi_\infty^2 = -\alpha/\beta$ (α is negative). The differential equation then simplifies to

$$\frac{\hbar^2}{2m|\alpha(T)|}\frac{d^2\Psi}{dx^2} + \Psi - \Psi^3 = 0. \tag{4.6}$$

The coefficient $\hbar/2m|\alpha(T)|$ is then identified as the squared characteristic length $\xi^2(T)$. This can be more evidently seen by linearising the above equation by setting $\Psi(x) = 1 + \chi(x)$ where $\chi(x) << 1$. We then obtain to first order in χ

$$\xi^2(T)\frac{d^2\chi}{dx^2} + (1+\chi) - (1 + 3\chi + \dots) = 0,$$

which simplifies to

$$\frac{d^2\chi}{dx^2} = \frac{2}{\xi^2}\chi. \tag{4.7}$$

The equation implies that deviations in ψ from ψ_∞ decay as $\sim e^{-\sqrt{2}x/\xi}$, that is over a characteristic length $\xi(T)$. More physically, $\xi(T)$ can be thought of as the length scale over which the magnitude of the order parameter can vary without excessively contributing to the free energy of the system.

The London limit mentioned above is applicable in systems where applied fields are weak, much lower than critical fields [111] such that no pair breaking occurs. Another motive for employing the limit is when the London penetration depth is much larger than the coherence length [122] and the electrodynamics can be treated in a local manner, as in London theory. This feature is present for example in cuprate superconductors as we will see in the next subsection. A slightly different but computationally similar limit is in applications where the fields are strong enough to partly deplete the superconducting condensate resulting in $|\psi| < \psi_\infty$ but where $|\psi|$ is uniform across the sample. This can occur in thin films or wires where the B-field is aligned such that the symmetry of the system would require $|\psi|$ to vary along a direction for which the thickness of the material is much smaller than the coherence length $d \ll \xi$. Any variation in $|\psi|$ within this distance would then come at too large an energy cost and the order parameter can be approximated as in the London limit by an expression of the form $|\psi|e^{i\phi(\mathbf{r})}$. The second GL equation is then reduced to

$$\mathbf{J} = \frac{e}{m}(\hbar\nabla\phi - 2e\mathbf{A})|\psi|^2. \tag{4.8}$$

We will use this expression in the next section to describe the electrodynamics of Josephson junctions and in Chapter 5 when we present a model for layered superconductors.

Because of the phenomenological nature of GL theory, its merit was not fully appreciated until nine years after it was first published, when Gor'kov showed that GL theory in fact follows from the microscopic BCS theory near T_c [123]. A major success of GL theory was that it provided the basis for explaining the difference in behaviour of type 1 and type 2 superconductors and allowing the distinction between the two types to be exactly quantified by the GL parameter κ, defined as the ratio between the London penetration depth and the coherence length λ/ξ. In 1957 Abrikosov showed that materials with $\kappa > 1/\sqrt{2}$ are superconductors of the second type and should exhibit a second order transition to the normal state upon increasing the external magnetic field as described above and depicted in figure 4.1. He further predicted that beyond the lower critical field H_{c1} the partial field penetration occurs in the form of a lattice of flux tubes, each carrying one quantum of magnetic flux [124]. Each flux tube is surrounded by a supercurrent vortex concentrating the magnetic flux at its centre, where the material reaches the normal state while outside the core it remains superconducting, hence termed the mixed state. The existence of these Abrikosov vortices as they came to be known was later confirmed by electron microscopy observations [125–127].

4.1.4 More on HTS and Cuprates

Cuprates were the first HTS to be discovered and have been the most extensively studied. They are quasi two-dimensional compounds and their general crystal structure consists of stacked planes of copper oxide separated by insulating layers in a repeating lattice, hence their alternative name: layered superconductors [2]. The insulating layers can all be identical in which case a unit cell of the structure contains only one copper oxide plane and the material is termed single-layered. A bilayer cuprate is formed when the structure contains two types of insulating

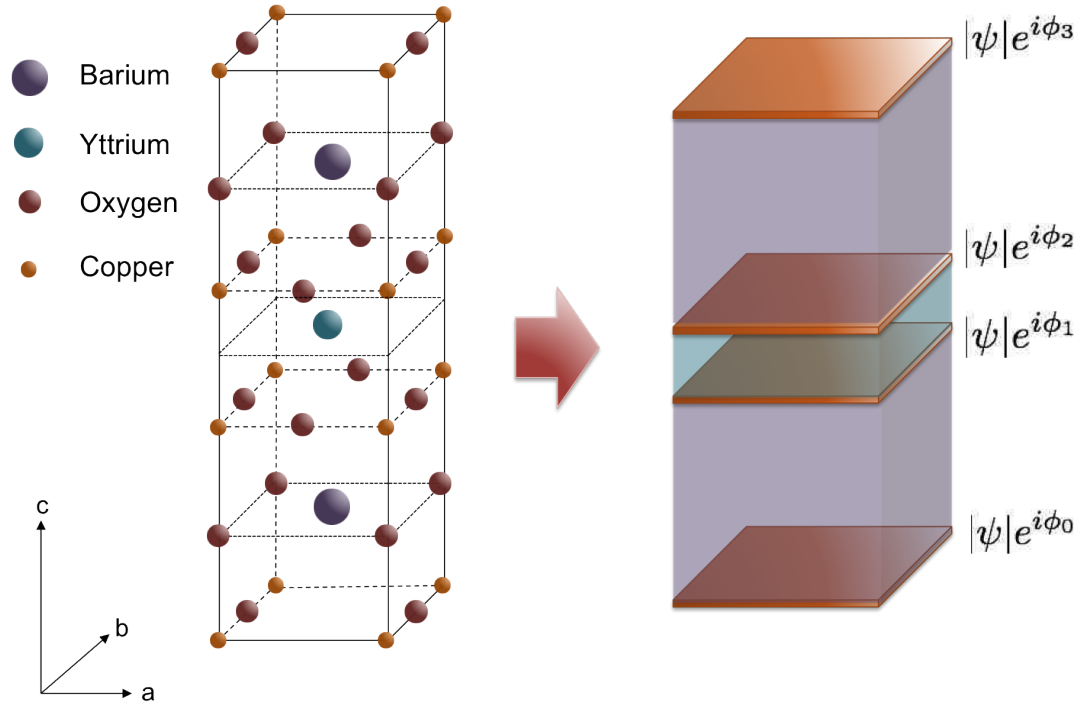


Figure 4.2: Left: Structure of YBCO an example of a bilayer cuprate superconductor where copper oxide planes of thickness ~ 0.1 nm are separated by insulating layers of ~ 10 nm [138]. The c-axis is oriented perpendicular to the CuO planes which are themselves parallel to the ab-plane. Right: Schematic of the material as a series of alternating superconducting copper oxide layers and insulating layers effectively modelled as a stack of Josephson junctions.

layers that repeat in an alternating pattern in the crystal. More complex multilayer structures can of course also exist. A prominent example of a bilayer cuprate is YBCO. As shown in figure 4.2 it is made up of insulating layers containing either barium or the rare earth element yttrium and is the type of compound we have in mind with regards to implementing the cooling scheme presented in this thesis.

The parent stoichiometric compounds of the cuprate HTS are antiferromagnetic Mott insulators, which then become superconducting upon doping[5]. Figure 4.3 shows a schematic phase diagram for a typical cuprate superconductor. Many theories were initially proposed to explain how high temperature superconductivity arises in cuprates but till date none of them provide a complete generalised

[5]They can either be electron or hole doped depending on the compound [9]. YBCO for example is hole doped.

microscopic description that can explain the all experimental evidence and that most scientists agree on [3]. Two main theories however have the most support. The first is the resonating valence bond theory, devised by P. Anderson [128] and attributes superconductivity in cuprates to their atomic structure. It argues that electrons from neighbouring copper atoms can form pairs via valence bonds which then become mobile and behave as cooper pairs as the material is doped. The other theory known as spin fluctuation instead holds antiferromagnetic correlations as responsible for electron pairing [129]. Unlike traditional BCS-type superconductors which exhibit an isotropic superconducting gap in momentum space (called s-wave superconductors), electron pairing in these novel superconductors display d-wave symmetry [130, 131]. Advancements in applications of HTS are however not solely reliant on the microscopic details and indeed a lot of progress has been made utilizing only macroscopic descriptions [120, 132]. There is concensus about certain features and electrodynamic properties of HTS.

For instance it is agreed that as in BCS type superconductors, superconducting transport occurs via paired electrons as showed by Gough *et al.* via the observation of magnetic flux occuring in quanta of $h/2e$ instead of h/e [133]. It is also recognised that unlike in conventional superconductors, fluctuations in the phase of the Ginzburg-Landau order parameter are important in determining the T_c. Emery and Kivelson [134] investigated the importance of such fluctuations by computing, from experimentally measured parameters, an upper bound T_θ^{max}, the temperature at which phase coherence is lost whilst ignoring fluctuations effects in other degrees of freedom. This was then compared to the actual values of T_c. While T_θ^{max}/T_c was of the order of 10^5 for pure metals indicating that phase fluctuations have a negligible effect on T_c the ratio was of the order of unity for hole doped superconductors like YBCO therefore indicating the opposite. Phase fluctuations were in fact found to be most significant in HTS of the lowest degree of hole doping (un-

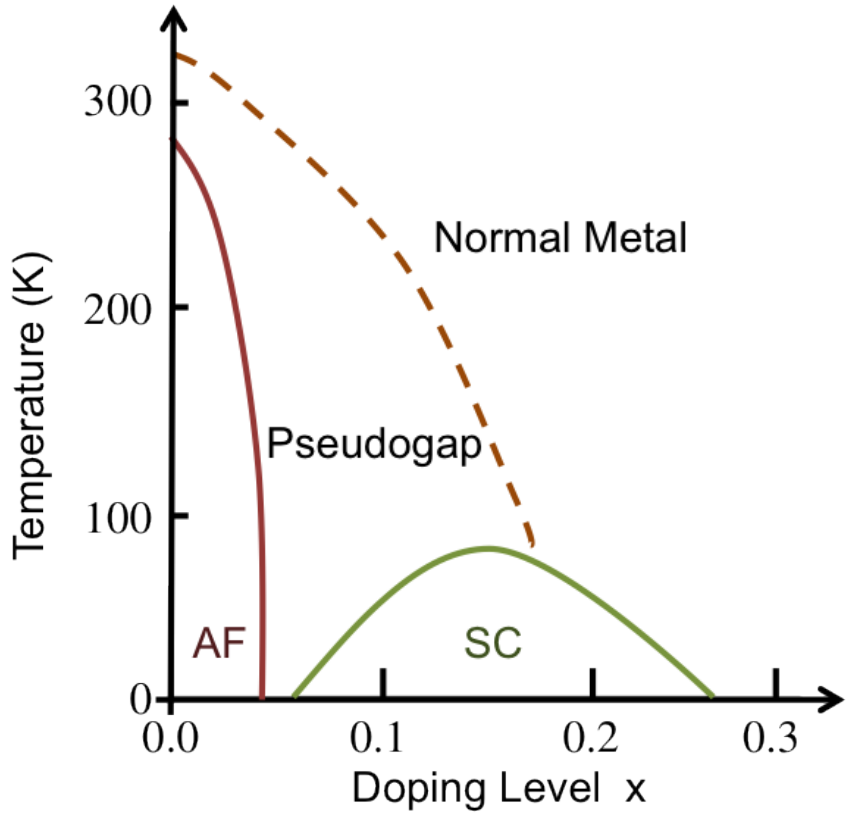


Figure 4.3: Schematic phase diagram for an HTS showing variations with temperature and level of hole doping. The undoped compound is antiferromagnetic (labelled AF) at low temperatures. This antiferromagnetism is destroyed as the material is hole doped. As the doping level increases a superconducting state (SC) emerges with the critical temperature peaking before eventually falling to zero as doping is further increased. At higher temperatures, the material is in the pseudogap or normal metal state.

derdoped compounds), since the low superfluid densities in such compounds means the phase is more sensitive to thermal energy fluctuations[6]. This feature is central to this thesis. Our proposed cooling scheme aims to enhance superconductivity by precisely targeting these thermal phase fluctuations. This concept is more clearly illustrated in the next section on Josephson junctions.

Today a wealth of experimental evidence supports the idea of modelling the

[6]The superfluid or condensate density determines the resistance of the phase to perturbations like those due to thermal energy fluctuations. This is most easily understood by considering the HTS in the Lawrence-Doniach model. The free energy density expression 4.10 makes clear the role of $|\psi|$ as a 'phase stiffness'.

electrodynamics of layered HTS by a stack of Josephson junctions [132, 135], with the copper oxide planes acting as the superconducting layers (see next section of Josephson junctions). The first such model used was the Lawrence-Doniach model [111]. It is similar to a discretised form of GL theory according to which the free energy of a superconducting system can be written as [111]

$$F = \sum_n \int \alpha|\psi_n|^2 + \beta|\psi_n|^4 + \frac{\hbar^2}{2m_{ab}}\left(\left|\frac{\partial\psi_n}{\partial x}\right|^2 + \frac{\partial\psi_n}{\partial y}\right|^2\right) + \frac{\hbar^2}{2m_c s^2}|\psi_n - \psi_{n-1}|^2, \quad (4.9)$$

where s is the distance between superconducting layers. The integral is in the ab-plane and the sum is over the copper oxide layers. The masses m_{ab} and m_c account for the different modes of charge transport along and between the layers respectively and reflect the material anisotropy [111]. Taking the GL order parameter to be $\psi_n = |\psi|e^{i\phi_n}$, the last term in the above equation reduces to

$$\frac{\hbar^2}{2m_c s^2}|\psi|^2(1 - \cos(\phi_n - \phi_{n-1})), \quad (4.10)$$

which has the exact form of the free energy of an ideal Jospehson junction computed by integrating the work done by an electrical source to change the phase difference between the two superconducting layers from zero to $\phi_n - \phi_{n-1}$.

The model has been successful in reproducing experimental observations of the frequency dependent reflectance [132] where for example Tamasaku *et al.* probed the interlayer dynamics with light polarised perpendicular to the oxide layers. Below T_c, they observed a sharp reflectivity edge in the c-axis spectrum at a frequency $\omega < 2\Delta$ suggesting the presence of an interlayer hopping energy $t < \Delta$ that could be explained by Josephson tunnelling. The values of intrinsic parameters in cuprates make these Josephson excitations occur at terahertz frequencies [132], and a c-axis Josephson plasma resonance was observed via terahertz time-domain

spectroscopy [137].

The Josephson coupled layer model has undergone further refinements to take into account additional coupling effects, largely due to the small thickness of the CuO layers. Recognising that the London penetration depth ($\sim$ 100 nm [138]) of the superconducting layers was much larger than their thickness ($\sim$ 0.1 nm [138]) and therefore that the B-fields from adjacent junctions are not perfectly screened from each other Sakai *et al.* proposed a model of inductively coupled junctions to encapsulate this feature [139]. A similar model was used by Kleiner and Müller in their extensive work on a range of cuprates where they demonstrated dc and ac Josephson effects, consistent with the theory [140].

A further development to the model was the addition of capacitive coupling [135]. Because the charge screening length is comparable to the superconducting layer thickness [141] E-field coupling between the intrinsic Josephson junctions in HTS also exists. Since the London penetration depth is much larger than the charge screening length, B-field coupling generally dominates and imperfect charge screening effects can often be ignored. As will be seen in Chapter 5 however, the size of the inductive coupling parameter depends on spatial variations of the order parameter phase in the ab-plane and vanishes in the short junction limit when ϕ is uniform the along superconducting layers. Capacitive coupling therefore cannot be neglected close to this limit. Such a scenario requires a unified model, that incorporates both effects [142].

The Doppler cooling scheme presented in this thesis requires such a model of layered superconductors, and will be outlined in Chapter 5. We shall refer back to points presented in this section when the validity of the model is discussed later. The next section introduces the Josephson physics required for modelling a bilayer cuprate.

4.2 Josephson Physics

The laws of quantum mechanics allow for particles to overcome classically unsurmountable energy barriers via quantum tunnelling. Electrons travelling between two conductors separated by a thin insulating gap are an example of a physical system where such a process occurs. In this case the work function of the conductor and the classical energy required for the electron to cross the insulating gap constitutes the energy barrier. Today, this effect is well understood and is exploited in a number of applications such as in electronic components like tunnel diodes or in imaging via the use of scanning tunnelling microscopes [143].

In 1962 B. D. Josephson predicted that a similar phenomenon can occur between two superconductors separated by an insulating barrier [144], a device now known as a Josephson junction. He found that superconducting electron pairs can tunnel between the two superconducting electrodes which, when not voltage biased results in a d.c supercurrent having a magnitude that depends on the difference in the phase of the superconducting Ginzburg-Landau order parameter across the barrier. His calculations also predicted that the phase difference evolves linearly with time when a constant electric potential difference is established between the two electrodes which in turn results in an alternating supercurrent flowing across the junction with a frequency proportional to the voltage across the junction.

These phenomena are now known as the d.c and a.c Josephson effects respectively. The former was confirmed by Anderson and Rowell in the year following Josephson's prediction when the authors reported an anomalous dc tunnelling current in tin oxide barriers between superconducting lead and tin electrodes which behaved as the Josephson current would be expected to [145]. The a.c Josephson effect on the other hand was verified indirectly through the observation of a resonance phenomenon known as Shapiro steps, which occur as a result of the form of

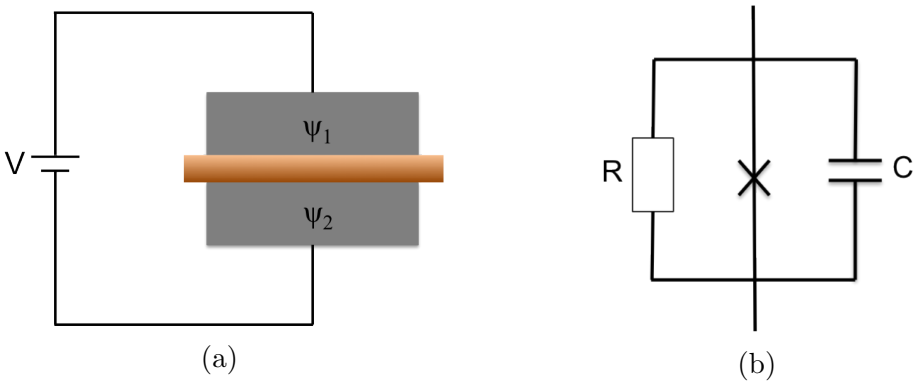
the supercurrent-phase relation [146].

Today Josephson junctions have found a number of applications one of the most notable of which is in Superconducting quantum interference devices (SQUIDs) used in precision metrology [147]. In addition, there has been extensive research exploring the use of Josephson junctions to implement qubits for quantum computing [148]. Developments have also been made towards the production of Josephson junction based microwave photon counters [149]. The non-linearity of the d.c Josephson relations and the ability for stacks of closely spaced junctions to couple to one another makes a wide range of dynamical behaviours possible [150]. One such example is the plasmonic behaviour exhibited by layered superconductors, which, as mentioned in the previous section are effectively dense stacks of homogeneous Josephson junctions and which can be exploited for practical applications such as the design of compact THz sources [138].

In this section we will first discuss the origin of the Josephson relations followed by the phase dynamics of real short junctions and introduce the concept of phase cooling. We then move on to treat long junctions in the presence of magnetic fields. The discussion is then continued in the next chapter where we begin by introducing a model for layered superconductors consisting of stacks of junctions.

4.2.1 Origin of the Josephson effect

Although the d.c and a.c Josephson relations were originally obtained from a microscopic analysis of superconducting systems partitioned by thin barriers [144,151, 152], their origin can be understood in a remarkably simple way in terms of coupled Schrödinger equations [153]. In this approach, presented by Feynman, we consider two superconductors connected by a layer of insulating material as shown in figure 4.4a with a voltage V applied across. If the insulating layer is too thick, supercon-



(a) (b)

Figure 4.4: (a): A Josephson junction made up of two superconductors separated by a thin insulating barrier. The charge supercarriers in each electrode are described by the complex order parameters ψ_1 and ψ_2. A voltage V is applied across the junction. (b): The RCSJ model describes a real junction as an ideal one shunted by a resistor R and a capacitor C to acccount for quasiparticle transport and charging effects respectively.

ducting electron pairs are not able to jump across the barrier. However if it is thin enough, there is a finite amplitude of a pair tunneling from one superconductor to the other. To analyse this system, we denote the probability amplitude of finding an electron pair on one side of the barrier by ψ_1 and the amplitude of finding it on the other side by ψ_2[7]. We also require that no magnetic field is present. In this case, the Schrödinger equation describing the two amplitudes can be written as

$$i\hbar\dot{\psi_1} = U_1\psi_1 + K\psi_2, \tag{4.11a}$$

$$i\hbar\dot{\psi_2} = U_2\psi_2 + K\psi_1, \tag{4.11b}$$

where K is real and is a characteristic coupling constant that depends on the junction parameters. It is this term that accounts for the possibility of electron pairs tunnelling between the superconducting electrodes. Without the coupling term, the above set of equations would describe two separated, non interacting superconductors with the superconducting electrons in their lowest energy states of energies U_1 and U_2 respectively.

[7]This is similar to the Ginzburg-Landau complex order parameter.

We proceed the analysis by writing ψ_1 and ψ_2 in the explicitly complex form

$$\psi_1 = \sqrt{\rho_1} e^{i\phi_1}, \tag{4.12a}$$

$$\psi_2 = \sqrt{\rho_2} e^{i\phi_2}. \tag{4.12b}$$

Substituting these into equations 4.11 and comparing the real and imaginary parts we obtain

$$\dot{\rho_1} = -\dot{\rho_2} = \frac{2K}{\hbar}\sqrt{\rho_1\rho_2}\sin(\phi_1 - \phi_2), \tag{4.13a}$$

$$\hbar(\dot{\phi_2} - \dot{\phi_1}) = U_1 - U_2. \tag{4.13b}$$

The first equation describes electron pair transfer from one superconductor to another and hence can be associated with a supercurrent I flowing across the barrier. If there is a voltage V applied across the junction, then $U_1 - U_2 = 2eV$, where $2e$ is the charge of an electron pair. Introducing the phase difference ϕ as $\phi = \phi_1 - \phi_2$, equations 4.13 can be recast as

$$I = I_c \sin(\phi), \tag{4.14a}$$

$$\dot{\phi} = \frac{2eV}{\hbar}, \tag{4.14b}$$

where I_c is proportional to $\frac{2K}{\hbar}\sqrt{\rho_1\rho_2}$ from equation 4.13 above and is called the critical current. It is the maximum supercurrent that the junction can support. Equations 4.14a and 4.14b describe the d.c and a.c Josephson effects respectively. If there is no voltage drop across the junction, a d.c supercurrent from anywhere between $-I_c$ to I_c can be made to flow across the junction. If on the other hand a voltage V is set up across the junction, the phase difference evolves in time as $\phi(t) = \phi(0) + \frac{2eV}{\hbar}t$. This in turn leads to an alternating supercurrent of amplitude

I_c that varies sinusoidally in time with frequency $\nu = 2eV/h$, hence where the a.c Josephson effect gets its name from.

It must be pointed out however that the Josephson relations written above hold only in the absence of magnetic fields. This is because unlike the supercurrent which is a well-defined gauge-invariant physical quantity, the phase difference is not. It does not have a unique value for a given physical situation while the supercurrent does and therefore cannot alone define the latter. A more involved treatment of the Josephson effects using the Ginzburg-Landau equations in the previous section reveals that a corrected gauge-invariant phase difference should instead be used in general cases [111] and is defined as

$$\gamma = (\phi_1 - \phi_2) + \frac{2e}{\hbar}\int_1^2 \mathbf{A}.\mathrm{d}l, \tag{4.15}$$

where $\mathbf{A}$ is the magnetic vector potential and integration is from one superconducting layer (1) to the other (2). More critically, this quantity also allows us to treat the effects of magnetic fields on the phase dynamics of junction. From this point on, we will use ϕ to denote the gauge invariant phase difference.

While the Josephson relations 4.14a and 4.14b are generally sufficient to describe the zero voltage physics of Josephson junctions, they fail to account for other physical phenomena occuring in real junctions such as dissipation via the tunnelling of quasiparticles under a voltage bias. Another aspect not accounted for is the fact that a Josephson junction, two extended superconductors separated by an insulating layer, has the physical structure of a capacitor and as such charging and discharging of the superconducting electrodes provide an additional contribution to the current that can flow through a real junction. These features are captured by the Resistively and Capacitively shunted junction (RCSJ) model which treats a real junction as an ideal one described by equations 4.14 connected in parallel

to a capacitor and a resistor (figure 4.4). The total current is then the sum of the capacitive, resistive and supercurrent contriutions giving[8]

$$I = I_c \sin\phi + \frac{V}{R} + C\frac{\mathrm{d}V}{\mathrm{d}t},$$

which using equation 4.14b gives

$$\frac{I}{I_c} = \sin\phi + \frac{\hbar}{2eRI_c}\frac{\mathrm{d}\phi}{\mathrm{d}t} + \frac{\hbar C}{2eI_c}\frac{\mathrm{d}^2\phi}{\mathrm{d}t^2}. \tag{4.16}$$

Introducing the dimensionless time variable $\tau = \omega_p t$ the above equation can be written as

$$\frac{I}{I_c} = \sin\phi + \beta\frac{\mathrm{d}\phi}{\mathrm{d}\tau} + \frac{\mathrm{d}^2\phi}{\mathrm{d}\tau^2}, \tag{4.17}$$

where $\omega_p = \sqrt{\frac{2eI_c}{\hbar C}}$ and is called the Josephson plasma frequency. It is the resonant frequency of oscillations of the phase difference in the absence of damping in the limit of small ϕ when $\sin\phi \approx \phi$. $\beta = 1/\omega_p RC$ and is the damping coefficient. As long as $I < I_c$, a static solution $\phi = \sin^{-1} I/I_c$ exists but when $I > I_c$ the junction switches to a dynamical state that includes dissipation.

4.2.2 Phase cooling

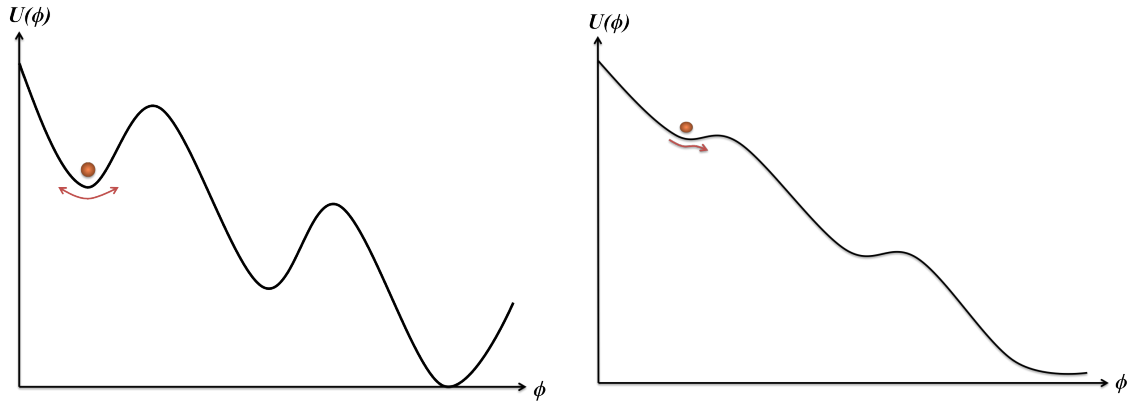
The dynamics can be more intuitively understood using a mechanical analogue known as the tilted washboard model. It turns out that the equation describing ϕ is the same as that of a particle of mass $(\hbar/2e)^2 C$ moving in a potential

[8]There are of course additional features that can be added to the model to simulate real junctions more accurately. One example would be to make the electrical resistance voltage dependent to account for an increase quasiparticle density resulting from pair breaking at high voltages [111]. We will however limit ourselves to this simpler model but nevertheless remain prudent with regards to the regime within which it is sufficient to do so.

$$U(\phi) = -\frac{\hbar}{2e}(I_c \cos\phi - I\phi), \tag{4.18}$$

where here ϕ represents the horizontal position coordinate of the particle. The particle also experiences a viscous drag of $\frac{\hbar^2}{4e^2R}\frac{\mathrm{d}\phi}{\mathrm{d}t}$. The bias current I affects the tilt of the potential. As long as $I < I_c$ the potential profile still has maximum and minimum points (see figure 4.5) and one can intuitively deduce that a possible low energy solution is one where the particle is stationary at one of the minima. This corresponds to the static solution $\phi = \sin^{-1} I/I_c$ mentioned above. As the current is increased, the potential minima become less and less deep until I reaches I_c where they become inflection points and the potential exhibits a continuous slope albeit of varying steepness (figure 4.5). When the bias current overshoots the critical current, for any set of initial conditions on ϕ, no static solution exists. In the mechanical analogue the general solution is one where the particle continuously moves down the potential slope, dissipating energy via viscous drag. It corresponds to the junction switching to a resistive lossy state. Purely superconducting transport therefore cannot be supported for currents exceeding the critical current.

In practice however, this switching to a dissipative regime occurs even before I_c is reached because of thermal fluctuations. Again, the mechanical analogue provides a conceptually useful way of understanding such effects. A Josephson junction coupled to a heat bath will experience random shifts in its free energy of the order k_BT, which translates to fluctuations in the phase difference. In the tilted washboard model this causes to and fro oscillations in the position of the particle about its equilibrium. If k_BT is of the order of the potential energy difference between a minimum and the next maximum, it is possible for the particle to overcome this energy barrier and jump to the next potential minimum. For a heavily damped system, the particle eventually settles at the next potential minimum since any



(a) (b)

Figure 4.5: (a) Particle moving in a washboard potential. When $I < I_c$ particle oscillates about a minimum due to thermal fluctuations (b) Shape of potential as I approaches I_c. Thermal fluctuations are more likely to allow the particle to overcome the now lower potential barrier resulting in a phase escape.

kinetic energy gained by the particle when moving down the potential is quickly dissipated by the viscous drag such that it does not possess enough energy to overcome the next potential barrier unless thermally excited once again. The result is a diffusive propagation of the particle over the potential barriers [111,154]. This is in contrast to the situation where damping[9] is minimal. In this case, once the barrier is overcome, because the particle loses hardly any energy via viscous drag, it will have enough kinetic energy to overcome the next potential barrier when it reaches the latter and can therefore continuously move down the potential, resulting in a thermally activated phase escape. The Josephson junction switches to and stays in a resistive state unless the bias current is reduced. The higher the temperature, the higher the energy barrier that can be overcome and consequently the smaller the bias current at which phase escapes can occur is. Reducing phase fluctuations therefore allows a larger current to run through the junction whilst still being in the superconductive state. In the context of HTS, reducing phase fluctuations thus

[9]This is the case we will be considering in this thesis to model layered superconductors.

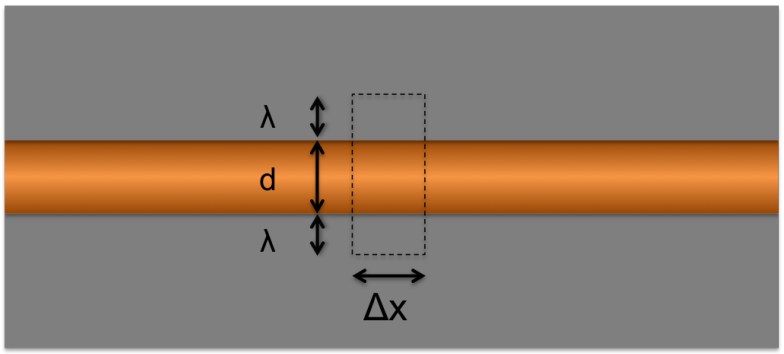


Figure 4.6: Schematic of extended Josephson junction with a barrier of thickness d. The direction of the B-field is taken to be into tha plane of the paper. λ is the London penetration depth of the superconducting electrodes.

enhances superconductivity.

4.2.3 Long Junctions

So far we have only considered the short junction limit where the phase difference was considered to be uniform along the length of an electrode. In fact, in the presence of magnetic fields ϕ can exhibit a spatial dependence. This together with the non-linearity of the Josephson junction allows for a rich set of behaviours of the phase difference. To derive the electrodynamics of long junctions, consider figure 4.6 which shows an extended junction in a magnetic field $\mathbf{B}$ taken to be into the plane of the paper. We first begin by integrating the magnetic vector potential along the contour shown in the figure. This must be equal to the magnetic flux through the area bounded by the contour. In addition, we can simplify the contour integral by noting that since the magnetic field is effectively screened by the superconducting electrodes within distances equal to the London penetration depth λ, the contribution of the horizontal sides of the rectangular contour can be neglected. We are then left with the expression

$$\int_s \mathbf{A}.\mathrm{d}l + \int_b \mathbf{A}.\mathrm{d}l \approx (2\lambda + d)B\Delta x, \tag{4.19}$$

where the subscripts s and b denote integration along the part of the contour within the superconducting electrodes and the barrier respectively. Using the definition of the gauge invariant phase difference and the Ginzburg-Landau equation 4.8, the above equation can be written as [111]

$$\phi(x + \Delta x) - \phi(x) \approx 2\pi(2\lambda + d)B\Delta x/\Phi_0, \tag{4.20}$$

where $\Phi_0 = h/2e$ is the magnetic flux quantum. In the limit of small Δx this reduces to

$$\frac{\partial \phi}{\partial x} = 2\pi(2\lambda + d)B/\Phi_0. \tag{4.21}$$

Now differentiating equation 4.21 w.r.t x and using Maxwell's equation

$$\nabla \times \mathbf{B} = \mu_0 \mathbf{J} + \mu_0 \epsilon_0 \epsilon \frac{\partial \mathbf{E}}{\partial t}, \tag{4.22}$$

we obtain

$$\frac{\Phi_0}{2\pi(2\lambda + d)} \frac{\partial^2 \phi}{\partial x^2} = \mu_0 J_z + \mu_0 \epsilon_0 \epsilon \frac{\partial E_z}{\partial t} \tag{4.23}$$

where the subscript z denotes the vertical coordinate in figure 4.6. Using the Josephson relations to substitute for J_z and E_z we arrive at the so called sine-Gordon equation [111, 152]

$$\frac{\partial^2 \phi}{\partial x^2} - \frac{1}{\tilde{c}^2} \frac{\partial^2 \phi}{\partial t^2} - \frac{\beta}{\tilde{c}^2} \frac{\partial \phi}{\partial t} = \frac{1}{\lambda_J^2} \sin \phi, \tag{4.24}$$

where $\tilde{c} = c/\sqrt{\epsilon(1 + 2\lambda/d)}$ is called the Swihart velocity, λ_J the Josephson penetration depth and β is the damping coefficient. The Jospehson penetration depth can be understood as follows. In the limit of small ϕ and ignoring the

damping and considering only static solution, the sine-Gordon reduces to a London type equation $\nabla^2\phi = -\phi/\lambda_J^2$. Therefore ϕ and hence the supercurrent is confined within the characteristic length λ_J from the junction edges.

Again taking the limit of small ϕ and neglecting the damping term, reduces the sine-Gordon equation to a wave equation. As such, plane wave solutions in ϕ of the form $\phi(x,t) = \phi_0 e^{i(kx-\omega t)}$ exist. They correspond to plasma wave oscillations and follow the dispersion relation $\omega^2 = \omega_J^2 + \tilde{c}^2k^2$ with $\omega_J = \tilde{c}/\lambda_J$ being the plasma frequency introduced in the RCSJ model. It is this regime that we will be treating in this thesis. Of course, the sine-Gordon equation being a non-linear partial differential equation, many more possible solutions exist. One such example is soliton solutions which occur in the highly non-linear regime [155]. The are usually categorised in two classes namely kinks or antikinks and breathers [156], where the breather is generally viewed as a kink-antiking pair. Solitons carry one quantum of magnetic flux and are therefore also called fluxons.

Having laid the foundations of Josephson physics, we can now proceed to describe a model for layered superconductors in terms of a stack of coupled extended junctions which will be the subject of the first part of the following chapter.

Chapter 5

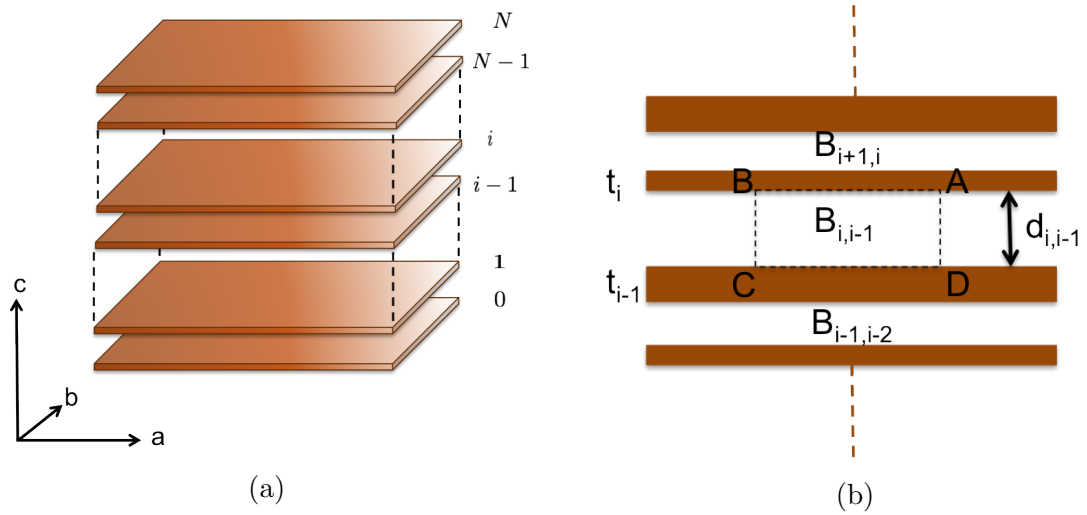
A Doppler Cooling Scheme for bilayer cuprates

5.1 The model

The cooling scheme we have in mind is intended for layered HTS having a bilayer structure. We begin by modelling one unit cell of these HTS as two stacked inductively and capacitively coupled Josephson Junctions. Our model closely follows that of Machida and Sakai [142].

We consider an arbitrary stack of Junctions with superconducting layers of varying thicknesses t_i and London penetration depths λ_i with the distance between layers labelled as $d_{i,i-1}$. The c-axis represents the direction perpendicular to the superconducting layers. For simplicity our junctions are taken to be extended along a and short b so that the phase difference between layers is assumed to be uniform along that latter direction (figure 5.1a).

We first consider the inductive coupling between the layers and begin by integrating the magnetic vector potential $\mathbf{A}$ around the loop ABCD shown in figure 5.1b applied to any arbitrary pair of junctions i and $i-1$. This integral is equal to the



(a) (b)

Figure 5.1: (a) shows an arbitrary stack of $N+1$ superconducting planes, each labelled i. The planes are taken to be extended in the a-direction and short in the b-direction along which the phase is assumed to be uniform. (b) A cross-section of a portion of the stack. Each superconducting layer has thickness t_i and the distance between layers i and $i-1$ is labelled $d_{i,i-1}$.

magnetic flux across the loop.

$$\oint \mathbf{A}.\mathrm{d}\mathbf{l} = \int \mathbf{B_{i,i-1}}.\mathrm{d}\mathbf{S} = \Phi. \tag{5.1}$$

Using the definition of the gauge invariant phase difference from equation which we rewrite here

$$\gamma = (\phi_1 - \phi_2) + \frac{2e}{\hbar}\int_1^2 \mathbf{A}.\mathrm{d}l,$$

and the expression for the current within superconducting layers from Ginzburg-Landau theory in the London limit

$$\mathbf{J}_i = -\frac{1}{2e\mu_0\lambda_i^2}\left(\hbar\nabla\theta_i + 2e\mathbf{A}_i\right),$$

we obtain

$$\frac{\partial \phi_{i,i-1}}{\partial x} = -\frac{2e}{\hbar} d_{i,i-1} B_{i,i-1} - \frac{2e\mu_0 \lambda_i^2}{\hbar} J_i^L + \frac{2e\mu_0 \lambda_{i-1}^2}{\hbar} J_{i-1}^U, \tag{5.2}$$

where the superscripts L and U refer to the lower and upper surfaces of a superconducting layer. From London's equations combined with Maxwell's equations for the B-field inside a superconductor we have

$$\frac{\partial^2 B_i}{\partial z^2} = \frac{1}{\lambda_i^2} B_i. \tag{5.3}$$

Solving the above with boundary conditions $\frac{\partial B}{\partial z} = \mu_0 \mathbf{J}$ enables us to express J_i^L and J_{i-1}^U in terms of the B fields in adjacent junctions with

$$J_i^L = \frac{1}{\mu_0 \lambda_i} \frac{B_{i,i-1} \cosh(t_i/\lambda_i) - B_{i+1,i}}{\sinh(t_i/\lambda_i)}, \tag{5.4a}$$

$$J_{i-1}^U = \frac{1}{\mu_0 \lambda_{i-1}} \frac{B_{i+1,i} - B_{i,i-1} \cosh(t_{i-1}/\lambda_{i-1})}{\sinh(t_{i-1}/\lambda_{i-1})}, \tag{5.4b}$$

we obtain

$$\frac{\hbar}{2e} \frac{\partial \phi_{i,i-1}}{\partial x} = d_{i,i-1}^L B_{i,i-1} + s_i^L B_{i+1,i} + s_{i-1}^L B_{i-1,i-2}, \tag{5.5}$$

with the effective magnetic thickness $d'_{i,i-1}$

$$d_{i,i-1}^L = d_{i,i-1} + \lambda_i \coth(t_i/\lambda_i) + \lambda_{i-1} \coth(t_{i-1}/\lambda_{i-1}), \tag{5.6}$$

and the coupling parameter s_i

$$s_i^L = -\frac{\lambda_i}{\sinh(t_i/\lambda_i)}. \tag{5.7}$$

Equation 5.5 describes how the phase difference $\phi_{i,i-1}$ across a particular junction depends on the magnetic field in the adjacent upper and lower junctions. This

is the origin of the inductive coupling we mentioned at the beginning of the chapter.

Machida and Sakai [142] formulated the electric field coupling using a semimicroscopic framework based on a Schrödinger equation for the macroscopic condensate wavefunction (the order parameter) which leads to an equation of similar form to 5.2 describing the coupling between adjacent Josephson junctions due to imperfect charge screening within the thin superconducting layers and is given by

$$\frac{\hbar}{2e}\frac{\partial\phi_{i,i-1}}{\partial t} = -\frac{\lambda_{c,i}^2}{\epsilon_i^s}\rho_i + \frac{\lambda_{c,i-1}^2}{\epsilon_{i-1}^s}\rho_{i-1} + \int_{i-1}^{i} E_z dz, \tag{5.8}$$

where λ_c is the charge screening length (Debye length), ρ_i is a superconducting layer charge density and ϵ_i^s the dielectric constant of the superconducting layer i. considering the variation of the scalar, chemical and electrochemical potentials across a junction, coupled with Maxwell's first equation [142], an expression for the electric field inside the superconducting layers is obtained and is given by

$$\frac{\partial^2 E_i}{\partial z^2} = \frac{1}{\lambda_{c,i}^2}E_i, \tag{5.9}$$

which is of the exact form as the London penetration of magnetic fields inside the superconductor. This enables us to import results already calculated above for inductive coupling with only minor adjustments to parameters needed. The capacitive coupling counterpart to equation 5.5 is then obtained as

$$\frac{\hbar}{2e}\frac{\partial\phi_{i,i-1}}{\partial t} = d_{i,i-1}^C E_{i,i-1} + s_i^C E_{i+1,i} + s_{i-1}^C E_{i-1,i-2}, \tag{5.10}$$

with $d_{i,i-1}^C$ and s_i^C similarly defined as

$$d_{i,i-1}^C = d_{i,i-1} + \lambda_{c,i}\coth\left(t_i/\lambda_{c,i}\right) + \lambda_{c,i-1}\coth\left(t_{i-1}/\lambda_{c,i-1}\right), \tag{5.11}$$

$$s_i^C = -\frac{\lambda_{c,i}}{\sinh\left(t_i/\lambda_{c,i}\right)}. \tag{5.12}$$

To demonstrate the cooling principle and for calculations in our preliminary feasibility study, we shall consider only one unit cell of the bilayer structure. For modelling one unit cell we have only two junctions made up of three superconducting layers which we label by the indices 0, 1 and 2. Physical quantities like the magnetic field in the insulating region between two superconducting layers will be labelled with subscripts "1,0" or "2,1", for example $B_{1,0}$ or $B_{2,1}$. Equations 5.5 and 5.10 can be formulated as

$$\frac{\hbar}{2e}\frac{\partial}{\partial x}\vec{\phi} = \mathbf{L}\vec{B}, \tag{5.13a}$$

$$\frac{\hbar}{2e}\frac{\partial}{\partial t}\vec{\phi} = \mathbf{C}\vec{E}, \tag{5.13b}$$

where $\vec{\phi}$, $\vec{B}$ and $\vec{E}$ are two dimensional column vectors describing the phase differences, magnetic fields and elecric fields across each junction. The matrices $\mathbf{L}$ and $\mathbf{C}$ are defined as

$$\mathbf{L} = \begin{pmatrix} d_{1,0}^L & s^L \\ s^L & d_{2,1}^L \end{pmatrix} \quad , \quad \mathbf{C} = \begin{pmatrix} d_{1,0}^C & s^C \\ s^C & d_{2,1}^C \end{pmatrix}. \tag{5.14}$$

By combining the above equations with the Maxwell equation for the insulating layers in one dimension which reads

$$\frac{\partial B_{i,i-1}}{\partial x} = \frac{\epsilon_{i,i-1}}{c}\frac{\partial E_{i,i-1}}{\partial t} + \mu_0 J_{i,i-1}, \tag{5.15}$$

we obtain an equation for the electrodynamics in terms of only the phase difference between layers given by

$$\frac{\hbar}{2e}\frac{\partial^2}{\partial x^2}\begin{pmatrix}\phi_{1,0}\\ \phi_{2,1}\end{pmatrix} = \mathbf{L}\left[\frac{\hbar\epsilon}{2ec^2}\,\mathbf{C^{-1}}\frac{\partial^2}{\partial t^2}\begin{pmatrix}\phi_{1,0}\\ \phi_{2,1}\end{pmatrix} + \mu_0\begin{pmatrix}J_{1,0}\\ J_{2,1}\end{pmatrix}\right], \tag{5.16}$$

where

$$J_{i,i-1} = \frac{\hbar\sigma_{i,i-1}}{2ed_{i,i-1}}\frac{\partial\phi_{i,i-1}}{\partial t} + J^c_{i,i-1}\sin\phi_{i,i-1}, \tag{5.17}$$

is the sum of the supercurrent and quasiparticle tunelling. $\sigma_{i,i-1}$ is the quasiparticle conductivity and $J^c_{i,i-1}$ is the critical current density of the particular junction. For the rest of our treatement we shall neglect the damping term caused by quasiparticle transport as in Denny *et al* [16].

Taking a London penetration depth, $\lambda_L \sim 100$ nm and a superconducting layer thickness, $d \sim 0.1$ nm along with a Debye length of $\lambda_D \sim 0.1$ nm which are of the correct order of magnitude for cuprate superconductors, we obtain $s_i^L/s_i^C \approx 10^6$. From equation 5.16, considering phase oscillations of the form $\phi = P\exp i(\omega t - kx)$ one can see that inductive coupling largely dominates as long as $kc/\omega > 10^{-3}$ which in fact occurs very close to zero k. Since we will be dealing with finite k and are only carrying a feasibility study, we shall neglect the fine details that the capacitive coupling brings into our equations of motion. From this point on we shall consider only inductive coupling to make calculations easier and tractable. In this regime, the equations defining the phase differences can be recast as

$$\frac{\partial^2\phi_{1,0}}{\partial x^2} = \alpha_1\frac{\partial^2\phi_{1,0}}{\partial t^2} + \Gamma_1\sin\phi_{1,0} + \Omega_2\frac{\partial^2\phi_{2,1}}{\partial x^2}, \tag{5.18a}$$

$$\frac{\partial^2\phi_{2,1}}{\partial x^2} = \alpha_2\frac{\partial^2\phi_{2,1}}{\partial t^2} + \Gamma_2\sin\phi_{1,0} + \Omega_1\frac{\partial^2\phi_{1,0}}{\partial x^2}, \tag{5.18b}$$

where $\alpha_1 = 1/\tilde{c}_i^2 = \mu_0\left(d^L_{1,0} - \frac{{s_1^L}^2}{d^L_{2,1}}\right)\frac{\epsilon_{1,0}}{d_{1,0}}$, $\Gamma_1 = \left(d^L_{1,0} - \frac{{s_1^L}^2}{d^L_{2,1}}\right)\frac{2\mu_0 e}{\hbar}J_{1,0_C}$ and $\Omega_1 = \frac{s_1}{d_{1,0^L}}$ and similarly for the terms with subscript '2'.

5.2 'Doppler' cooling scheme

In the limit of small ϕ (linearizing the sine in the supercurrent term), our coupled equations for the phase difference have plane wave solutions of the form

$$\phi_{1,0} = A \exp i(\omega t - kx), \tag{5.19a}$$

$$\phi_{2,1} = B \exp i(\omega t - kx). \tag{5.19b}$$

Substituting into the equation of motion, we find that they have a dispersion relation given by

$$\omega^2(k) = (\omega_{J1}^2 + \omega_{J2}^2) + (\tilde{c}_1^2 + \tilde{c}_2^2)k^2 \pm \sqrt{((\omega_{J1}^2 - \omega_{J2}^2) + (\tilde{c}_1^2 - \tilde{c}_2^2)k^2)^2 + 4\Omega_1\Omega_2\tilde{c}_2^2\tilde{c}_1^2k^4}, \tag{5.20}$$

where $\omega_{J1}^2 = \frac{2e}{\hbar}\frac{d_{1,0}}{\epsilon_{1,0}}$ is square of the bare plasma frequency of junction {1,0} and similarly for junction {2,1}. Typical order of magnitudes of the parameters occuring in cuprates are as follows: $\omega_J \sim 1$ THz, $\tilde{c}_i \sim c/10$ where c is the speed of light and $\Omega_i \sim 0.5$.

A plot of the dispersion curves is shown in figure 5.2 using typical parameters for a cuprate superconductor [140]. Two modes exist: a lower energy mode (shown in blue in figure 5.2 in which the phases oscillate in synchrony in both junctions, and a higher energy mode (shown in red) in which the phase difference across the two junctions are in antiphase. At a finite temperature T and for systems where the higher energy mode has a minimum frequency $\hbar\omega \gg k_BT$, only the lower energy plasmon is thermally excited up to k-values such that $\hbar\omega(k) \sim k_BT$. As depicted in the figure we could excite a travelling plasma wave from the lower energy to the higher energy mode using a counterpropagating laser beam. The momemtum imparted via the transition brings the plasma wave to a lower k-value. Subsequent

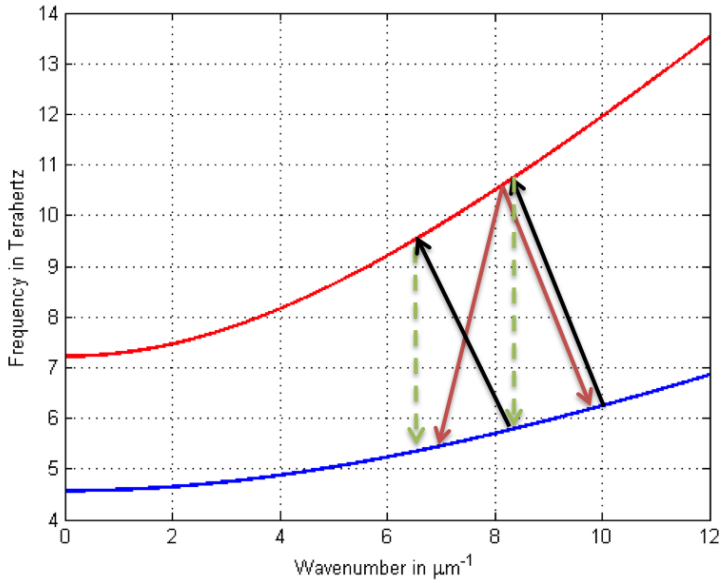


Figure 5.2: Dispersion of plane waves in the junctions using typical parameters for bilayer HTS with the higher energy mode in red and lower energy mode in blue. Laser induced transitions between the two modes are represented by the black arrows and the red arrows represent the two subsequent spontaneous decay paths with the green broken arrow showing that on average spontaneous decay approximately imparts zero momentum.

spontaneous decay to the lower mode on average imparts zero momentum. We can imagine repeating the process and bring plasmons to virtually zero k, thus extracting energy from the phase degree of freedom hence cooling it. The process at the same time restricts the phase excitations to having no spatial dependence along the length of the juction thereby effectively acting as the short junction described by Denny *et al* [16]. In other words, this presented scheme cools fluctuations along the a-b plane, a complementary process to the c-axis cooling of Denny *et al* [16].

The technique essentially works in the same way as Doppler cooling of atoms. Here the two modes act as the internal electronic states of the atoms. While in the atomic case Doppler shift changes the resonant absorption frequency depending on the velocity of the atom in the lab frame, in this case the dispersion relation dictates what the resonant frequency for a transition would be depending on the wavenumber k. Further developing this Doppler scheme requires working out whether these

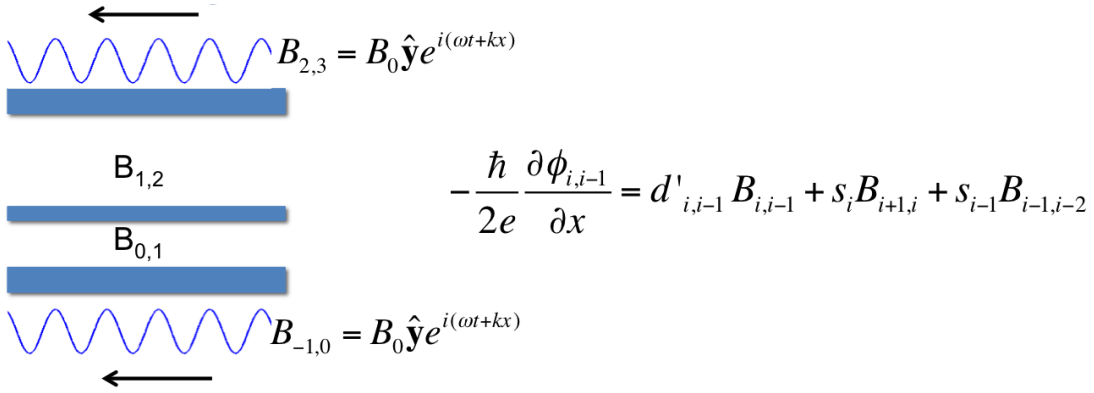


Figure 5.3: Schematic showing how the phase is driven in our model by an externally applied magnetic field via penetration through the upper and lower superconducting layers.

transitions between modes are in fact allowed, how strongly the system couples to the applied laser field and other relevant parameters like the Doppler cooling limit. This is discussed in more detail in the following sections.

5.3 Driving transitions

This section describes the work carried out to investigate whether it is possible to excite one plasmon from the lower energy to the higher energy mode by driving the system with an external electromagnetic (EM) field.

Our first attempt at modelling the interaction of the phase with an applied laser field considered only the effects of the B-field of the external EM field on the phase dynamics. We assumed that phase driving only occurs via the B-fields above and below the junctions due to imperfect screening by the superconducting layers (see figure 5.3). The effect of this external field on the phase difference across the junctions may be computed using equation 5.5 which has been reproduced in figure 5.3. This gave the following equation for the driven phase dynamics. Note from this point, for simplicity we will refer to the phase differences $\phi_{1,0}$ and $\phi_{2,1}$ across the junctions as ϕ_1 and ϕ_2 respectively.

$$\frac{\hbar}{2e\mu_0}\frac{\partial^2}{\partial x^2}\begin{pmatrix}\phi_1\\ \phi_2\end{pmatrix} = \begin{pmatrix} d_{1,0}^L & s_1^L \\ s_1^L & d_{1,0}^L\end{pmatrix}\begin{pmatrix} J_{c1}\sin\phi_1 + \alpha_1\frac{\partial^2\phi_1}{\partial t^2} \\ J_{c2}\sin\phi_2 + \alpha_2\frac{\partial^2\phi_2}{\partial t^2}\end{pmatrix} - kB\sin(kx+\omega t)\begin{pmatrix} d_{1,0}^L + 2s_1^L \\ d_{2,1}^L + 2s_1^L\end{pmatrix}. \tag{5.21}$$

Since the coupling is only linear, transitions from one mode to another which are essentially 3-photon processes are not allowed. Only two-photon processes can occur, corresponding to creation or annihilation of a particular excitation within a mode.

Insight from [27] lead us to realise that applying a bias current to the junctions shifts the average phase difference from zero to a finite value, thereby introducing a finite quadratic term in ϕ in our equations of motion for small phase fluctuations. This provides the non-linear term we need for 3-photon processes. The equation for one of the phase differences is given below as

$$\begin{aligned}\frac{\partial^2\phi_1}{\partial x^2} = {} & \frac{\omega_{J1}^2}{c_1^2}\left(\cos\Phi_1\phi_1 - \frac{sin\Phi_1}{2}\phi_1^2\right) + \frac{1}{c_1^2}\frac{\partial^2\phi_1}{\partial t^2} \\ & + \Omega_2\left(\frac{\omega_{J2}^2}{c_2^2}\left(\cos\Phi_2\phi_2 - \frac{sin\Phi_2}{2}\phi_2^2\right) + \frac{1}{c_2^2}\frac{\partial^2\phi_2}{\partial t^2}\right) \\ & + \frac{2e\mu_0 kB}{\hbar}(d_{1,0}^L + 2s_1^L)\sin(kx+\omega t),\end{aligned} \tag{5.22}$$

where Φ_1 and Φ_2 are the average phase differences across the two junctions due to the bias current and are assumed to be small so that the system only slightly deviates from the linearized case, hence allowing us to make the approximations that will follow. Within this model, due to imperfect shielding of magnetic fields by the thin superconducting layers, an externally applied field can drive currents along the superconducting plane, which translates to a quadratic driving of the phase. For simplicity we consider the artificial situation where we initially have only two modes present in the junction, one in phase mode (ω_-, k_1) and one antiphase mode

(ω_+, k_2) being driven by an applied field (ω_3, k_3).

We can write the following expression for the phase differences as an ansatz

$$\begin{pmatrix} \phi_1 \\ \phi_2 \end{pmatrix} = a(t)\mathbf{v}_-(k_1)e^{(i\omega_-(k_1)t-k_1x)} + b(t)\mathbf{v}_+(k_2)e^{(i\omega_-(k_2)t-k_2x)} + c(t)\mathbf{v_d}(k_3)e^{(i\omega_d(k_3)t-k_3x)}, \tag{5.23}$$

where '$\pm$' denote the higher and lower energy mode and $\mathbf{v_i}$ is the corresponding eigenvector for a particular mode. This expression can then be substituted to work out the evolution of the relative amplitudes $a(t)$ and $b(t)$ of the lower energy and higher energy modes respectively. After some algebraic manipulations we arive at

$$\ddot{a}(t) + 2i\omega_-(k_1)\dot{a}(t) = \Omega_a^2\ b(t)\ c(t)\ e^{-i\delta t}, \tag{5.24}$$

$$\ddot{b}(t) + 2i\omega_+(k_2)\dot{b}(t) = \Omega_b^2\ a(t)\ c(t)\ e^{i\delta t}, \tag{5.25}$$

on the condition that $\delta(k_2 + k_3 - k_1)$ and where $\delta = \omega_d - (\omega_+ - \omega_-)$ are reassuringly statements of conservation of momentum and energy respectively for the process, which is what we would expect. Ω_a^2 and Ω_b^2 are related via

$$\frac{\Omega_b^2}{\omega_+} = \frac{\Omega_a^2}{\omega_-} = \Omega, \tag{5.26}$$

and are rather lengthy expressions in terms of parameters of the junctions and the eigenvectors of the moved involved. Writing a particular eigenvector as

$$\mathbf{v_i} = \begin{pmatrix} \alpha_i(k) \\ \beta_i(k) \end{pmatrix}, \tag{5.27}$$

Ω_b^2 for example is given by the expression

$$\Omega_b^2 = \frac{\frac{\omega_{J1}^2}{\tilde{c_1}^2}\frac{\sin\Phi_1}{2}\alpha_-(k_1)\alpha_d + \Omega_2\frac{\omega_{J2}^2}{\tilde{c}^2}\frac{\sin\Phi_2}{2}\beta_-(k_1)\beta_d}{\frac{\alpha_+(k_2)}{\tilde{c}_1^2} + \frac{\Omega_2\beta_+(k_2)}{\tilde{c}_2^2}} \tag{5.28}$$

We shall now proceed to make two approximations to equations 5.25. First, we will assume that $c(t)$ is larger than $a(t)$ and $b(t)$ so that variations in c can be neglected and we approximate it by a constant. We also make the slowly-varying-envelope-approximation (SVEA), common in classical Bloch descriptions of oscillators which consists of ignoring the second order time derivative based on the assumption that the system is weakly enough driven such that the amplitudes $a(t)$ and $b(t)$ vary on timescales much longer than $1/\omega_\pm$. In this case the equations governing the amplitudes $a(t)$ and $b(t)$ reduce to the well known form

$$i\dot{a}(t) = \frac{\Omega}{2}\, b(t)\, e^{-i\delta t}, \tag{5.29}$$

$$i\dot{b}(t) = \frac{\Omega}{2}\, a(t)\, e^{i\delta t}, \tag{5.30}$$

reminiscent of the equations governing the probability amplitudes in a two level atom interacting with a laser field (Chapter 3). It is clear therefore that transitions between the two phase oscillation modes can be induced in the same way as excitation between energy levels between atoms.

5.4 Doppler cooling limit

The mathematical equivalence of our model with the atomic case means we can in principle apply the exact same framework for treating Doppler cooling in superconducting systems. Indeed, defining

$$u = ab^* + a^*b, \tag{5.31}$$

$$v = iab^* - ia^*b, \tag{5.32}$$

$$w = aa^* - bb^*, \tag{5.33}$$

and accounting for spontaneous decay phenomenologically by adding damping terms to the population differences and coherences, we obtain Classical Bloch equations of the exact form as the optical ones.

$$\dot{u} = \delta v - \frac{\Gamma}{2}u, \tag{5.34}$$

$$\dot{v} = -\delta u + \Omega w - \frac{\Gamma}{2}v, \tag{5.35}$$

$$\dot{w} = -\Omega v - \Gamma(w - 1). \tag{5.36}$$

This means that the exact same treatment we used for atoms can be applied here with only one difference. Whilst in the atomic case we wanted to find the minimum kinetic energy of the atom, here we want to find the minimum energy as per the dispersion relation. In the limit of small k, the dispersion relation for the lower energy mode may be approximated as

$$\omega_-(k) = \omega_{J1} + \frac{\tilde{c}^2 k^2}{\omega_{J1}}. \tag{5.37}$$

As with the atomic case, the equation describing the time dependence in k^2 takes the form

$$\frac{d\bar{k}^2}{dt} = 2Rk_r^2 - \gamma\bar{k}^2, \tag{5.38}$$

giving a limit on $\hbar\frac{\tilde{c}^2k^2}{\omega_J}$ of $\hbar\Gamma_{spont}/2$, where Γ_{spont} is the spontaneous decay rate

which we need to calculate. We have calculated this following [90] where we solve the equations for the amplitudes in the presence of broadband radiation to get a value for the Einstein B coefficient. Then using the relationship between the Einstein A and B coefficients

$$A_{21} = \frac{g_1}{g_2}\frac{\hbar\omega^3}{\pi^2 c^3} B_{12}, \tag{5.39}$$

we arrived at an expression for A_{21} as

$$A_{21} = \frac{\Omega_b^2 \alpha^2}{\epsilon_0(\delta + \omega_+)^2}\frac{\hbar\omega^3}{\pi c^3}, \tag{5.40}$$

resulting in a lifetime against spontaneous decay of ~ 100 ps. This therefore implies a Doppler cooling limit of ~ 0.1 K.

5.5 Validity of the treatment

At this point it is good to recap the important assumptions we have made so far. First of all, for this model we have in mind superconductors in which the phase fluctuations plays a crucial role in determining T_c such as underdoped YBCO. We have presented our model in the London limit, that is we have assumed that fields are small enough so that there is no depletion of the superconducting condensate via pair breaking. Concerning calculations presented for the Doppler cooling itself, we have employed the SVEA, which requires that the B-field be small enough so as not to induce rapid changes in the amplitudes $a(t)$ and $b(t)$. This approximation does not clash with the one above. Finally, we have treated the Doppler cooling mechanism entirely classically. Recall that we mentioned in Chapter 3 that it is only possible to treat changes in the velocity of the atom and here changes in k in the continuous limit only if the recoil due to one photon does not severely disrupt

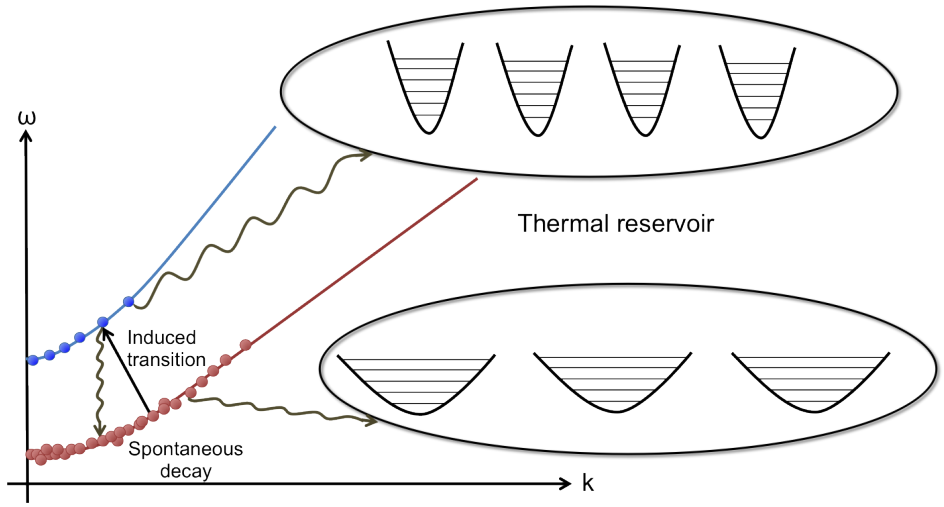


Figure 5.4: Diagram illustrating the bigger picture. The phase excitations are not only coupled to each other but also to other degrees of freedom. These can be thought of as being coupled to thermal baths of oscillators.

the resonance condition. The effective mass of the system considered here, coupled with the relatively low terahertz frequency driving and hence the small changes in k in each absorption event make this limit true in this situation and hence our treatment remains valid.

5.6 Reheating

In our above treatment, we have implicitly taken our system to be a two level one, with only two modes for plasmon excitations. However, in real materials, several other degrees of freedom are present, which are completely ignored here. As such, there exists several possible decay channels for phase excitations. The lifetime of 100 ps we have calculated above is against spontaneous decay via only one of the numerous possible decay routes, like via coupling to phonon modes in the material. Due to these other possible processes, the actual lifetime of the excited state is in fact about an order of magnitude smaller that the calculated value here [132]. Conversely the phase degree of freedom can be excited due to coupling to these

modes. As a result, unlike an atomic system, which is completely isolated, the phase degree of freedom can be rethermalised as it is effectively coupled to an outside environment at a typically higher temperature. In reality therefore, the effective Doppler cooling limit will be higher than the one calculated above as there will be reheating processes in direct competition with the cooling. This can be taken into account by adding a heating rate Q in our equation determining the cooling limit giving

$$\frac{d\bar{k}^2}{dt} = 2Rk_r^2 - \gamma\bar{k}^2 + Q, \tag{5.41}$$

which would increase the equilibrium $\bar{k}$ and hence effective cooling limit. This effective reheating rate would however have to be calculated by other means. A more detailed treatment would involve considering each mode as coupled to a thermal bath of oscillators as shown in figure 5.4 and adopting a Langevin approach similar to the one used by Denny *et al.* [16].

The findings of this chapter as well as a summary of the thesis are given in the next chapter.

Chapter 6

Summary and Outlook

In this thesis we have presented recent developments in the dynamical control of matter with light, with special emphasis on the improved experimental capabilities in coherently driving a single degree of freedom, with the Jospehson plasma in cuprates as example. Chapter 2 gave a short account of the technological advancements made in terahertz sources, the frequency at which Josephson excitations occur in cuprates. We showed how devices like the quantum cascade laser showed promise as a relatively compact and highly tunable source of moderately high power terahertz radiation, thus making the experimental realisation of coherent control of Josephson plasmas a realistic target for the near future. In Chapter 3 we outlined the physics behind the Doppler cooling in atomic systems, with a view of developing a counterpart for the phase of the order parameter in bilayer cuprates. This phase, as we argued in Chapter 4 can be the crucial in determining the critical temperature of the superconductive transition in underdoped cuprates. In that same chapter, we presented experimental evidence for modelling cuprates as a stack of coupled Josephson junctions to model their electrodynamics and introduced the physics required to construct such a model, namely the London and Ginzburg-Landay theories and basic Josephson physics.

By modelling one unit cell of a bilayer cuprate as two coupled junctions, we have shown that their phase dynamics, consisting of two oscillation modes is suitable for the implementation of a Doppler cooling scheme. Transitions between the two modes have also been shown to be possible by means of a quadratic coupling between the driving field and the phase oscillations, activated only in the presence of a bias current. Ignoring all other processes (assuming a two level system) we have an estimated a Doppler cooling limit of the order of 0.1 K, indicating that the inherent features of the cooling mechanism in cuprates are unlikely to be the limiting factor in determining the lowest temperature that can be reached. The effective cooling limit is rather likely to be determined by the competition between cooling and rethermalisation.

While we mentioned from the outset that this scheme was envisaged as a complementary process to the parametric cooling proposed by Denny *et al.* [16] for short juctions, a way of actually executing both schemes simultaneously in practice is not evident. The experimental conditions required for the two are different. The parametric cooling scheme proposes to excite vibrational modes in the lattice to act as a transducer of plasma frequencies, under no bias current, whereas our proposed scheme directly targets Josephson plasma excitations and requires a bias current, making the experimental compatibility of the two schemes questionable. A possible research direction for the future might therefore be to find cooling mechanisms that are compatible with either of the ones mentioned.

While the experimental demonstration of cooling in a single extended Josephson junction by Hammer and Aprilli [27] is certainly promising, it remains to be seen whether equally successful results will be achievable experimentally in the stacked systems of microscopic junctions offered by cuprates. If not, perhaps these cooling schemes could find use in artificially designed heterosctuctures.

Bibliography

[1] J. G. Bednorz and K. A. Müller, "Possible high T_c superconductivity in the Ba-La-Cu-O system." Z. Phys. B 64, 189 (1986).

[2] B. Keimer, S. A. Kivelson, M. R. Norman, S. Uchida and J. Zaanen, "From quantum matter to high-temperature superconductivity in copper oxides." Nature. 518, 179 (2015).

[3] A. Mann, "High-temperature superconductivity at 25: Still in suspense." Nature 475, 280 (2011).

[4] E. Dagotto, "Correlated electrons in high-temperature superconductors." Rev. Mod. Phys 66, 763 (1994).

[5] J. Bardeen, L. N. Cooper and J. R. Shrieffer, "Theory of superconductivity." Phys. Rev. 108, 1175 (1957).

[6] J. R. Gavaler, "Superconductivity in Nb-Ge films above 22K." Appl. Phys. Lett. 23, 480 (1973).

[7] J. Muller, "A15-type superconductors." Rep. Prog. Phys. 43, 641 (1980).

[8] M. K. Wu *et al.*, " Superconductivity at 93 K in a New Mixed-Phase Y-Ba-Cu-0 Compound System at Ambient Pressure." Phys. Rev. Lett. 58, 908 (1987).

[9] P. A. Lee, N. Nagaosa and X. Wen, "Doping a Mott insulator: Physics of high-temperature superconductivity." Rev. Mod. Phys 78, 17 (2006).

[10] A. Schilling, M. Cantoni, J. D. Guo and H. R. Ott, "Superconductivity above 130 K in Hg-Ba-Ca-Cu-O system." Nature 363, 56 (1993).

[11] C. W. Chu *et al.*, "Superconductivity above 150 K in $HgBa_2Ca_2Cu_3O_{8+\delta}$ at high pressures." Nature 365, 323 (1993).

[12] A. P. Drozdov, "Conventional superconductivity at 203 kelvin at high pressures in the sulfur hydride system." Nature 525, 73 (2015).

[13] Y. Seguchi, T. Tsuboi and T. Suzuki, "Magnetic-field-enhanced superconductivity in alloy films of Au-Ge." J. Phys. Soc. Jpn 62, 2564 (1993).

[14] H. A. Radovan *et al.*, "Magnetic enhancement of superconductivity from electron spin domains." Nature 425, 51 (2003).

[15] H. J. Gardner *et al.*, "Enhancement of superconductivity by a parallel magnetic field in two-dimensional superconductors." Nature Phys. 7, 895 (2011).

[16] S. J. Denny *et al.*, "Proposed parametric cooling of bilayer cuprate superconductors by terahertz excitation." Phys. Rev. Lett 114, 137011 (2015).

[17] K. Miyano, T. Tanaka, Y. Tomioka, and Y. Tokura "Photoinduced Insulator-to-Metal Transition in a Perovskite Manganite." Phys. Rev. Lett 78, 4257 (1997).

[18] M. Chollet *et al.*, "Gigantic Photoresponse in 1/4-Filled-Band Organic Salt $(EDO-TTF)_2PF_6$." Science 307, 87 (2005).

[19] A. Subedi, A. Cavalleri and A. Georges, "Theory of nonlinear phononics for coherent light control of solids." Phys. Rev. B 89, 220301 (2014).

[20] M. Rini *et al.*, "Control of the electronic phase of a manganite by mode-selective vibrational excitation." Nature (London) 449, 72 (2007).

[21] D. Fausti *et al.*, "Light-Induced Superconductivity in a Stripe-Ordered Cuprate." Science 331, 189 (2011).

[22] S. Kaiser *et al.*, "Optically induced coherent transport far above Tc in underdoped $YBa_2Cu_3O_{6+}$." Phys. Rev. B 89, 184516 (2014).

[23] W. Hu *et al.*, "Optically enhanced coherent transport in $YBa_2Cu_3O_{6.5}$ by ultrafast redistribution of interlayer coupling." Nat. Mater. 13, 705 (2014).

[24] A. Dienst *et al.*, "Optical excitation of Josephson plasma solitons in a cuprate superconductor." Nat. Mater. 12, 535 (2013).

[25] A. Dienst *et al.*, "Bi-directional ultrafast electric-field gating of interlayer charge transport in a cuprate superconductor." Nat. Photonics 5, 485 (2011).

[26] M. Aspelmeyer, T. J. Kippenberg and F. Marquardt, "Cavity optomechanics." Rev. Mod. Phys. 86, 1391 (2014).

[27] J. Hammer, M. Aprili *et al.*, "Microwave Cooling of Josephson Plasma Oscillations." Phys. Rev. Lett 107, 017001 (2011).

[28] P. H. Siegel, "Terahertz technology." IEEE Trans. Microwave Theory Technol. 50, 910928 (2002).

[29] D. H. Auston, K. P. Cheung, J. A. Valdmanis & D. A. Kleinman, "Cherenkov radiation from femtosecond optical pulses in electro-optic media." Phys. Rev. Lett. 53, 15551558 (1984).

[30] Ch. Fattinger, & D. Grischkowsky, "Point source terahertz optics." Appl. Phys. Lett. 53, 14801482 (1988).

[31] D. Grischkowsky, S. Keiding M. van Exter & Ch. Fattinger, "Far-infrared time-domain spectroscopy with terahertz beams of dielectrics and semiconductors." J. Opt. Soc. Am. B 7, 20062015 (1990).

[32] M. Tonouchi, "Cutting-edge terahertz technology." Nature Photon. 1, 97105 (2007).

[33] B. Ferguson and X. Zhang, "Materials for terahertz science and technology." Nature Materials, 1, 2633 (2002).

[34] J.Lusakowski et al., "Voltage tuneable terahertz emission from a ballistic nanometer InGaAs InAlAs transistor." Journal of Applied Physics 97, 064307 (2005).

[35] M. S. Shur and J. Q. Lu , "Terahertz sources and detectors using two-dimensional electronic fluid in high electron-mobility transistors." IEEE Trans. Microwave Theory Technol. 48 7506 (2000).

[36] A. El Fatimy *et al.*, "AlGaN/GaN high electron mobility transistors as a voltage-tunable room temperature terahertz sources." J. Appl. Phys. 107 024504 (2010).

[37] S. Perez, T. Gonzalez, D. Pardo and J. Mateos, "Terahertz Gunn-like oscillations in InGaAs/InAlAs planar diodes." J. Appl. Phys. 103 094516 (2008).

[38] H. Eisele, C. C. Chen, G. O. Munns, G. I. Haddad, "The potential of InP IMPATT diodes as high-power millimeter-wave sources: first experimental results." IEEE MTT-S Int Microwave Symp Digest 2:529532 (1996).

[39] A. Acharyya, & J. P. Banerjee, "Prospects of IMPATT devices based on wide bandgap semiconductors as potential terahertz sources." Applied Nanoscience, 4(1), 1-14 (2014).

[40] F. Maiwald, S. Martin, J. Bruston, A. Maestrini, T. Crawford, and P.H. Siegel, "2.7 THz waveguide tripler using monolithic membrane diodes." IEEE MTT-S Int. Microw. Symp. Dig., vol. 3, pp. 16371640 (2001).

[41] A. Maestrini *et al.*, "Design and Characterization of a Room Temperature All-Solid-State Electronic Source Tunable From 2.48 to 2.75 THz." IEEE Trans. THz Sci. Tech., vol. 2, no. 2, pp. 177-185 (2012).

[42] J.H. Booske *et al.*, "Vacuum Electronic High Power Terahertz Sources." IEEE Transactions on Terahertz Science and Technology, vol. 1, no. 1, pp. 54-75 (2011).

[43] R. Kompfner*et al.*, "Backward-wave tubes." Proc. IRE. Vol. 41, No.11, pp. 1602-1611, (1953).

[44] J. E. Walsh, J. H. Brownell, M. J. Goldstein, J. C. Swartz, J. Urata, and M. F. Kimmitt, "A new tunable coherent FIR-THz source." Opt. Photon. News, vol. 9, no. 12, pp. 5152, (1998).

[45] R. E. Miles, J. Garcia, J. R. Fletcher, D. P. Steenson, J. M. Chamberlain, C. M. Mann, and E. J. Huq, "Modeling of micromachined klystrons for terahertz operation." 8th Int. Terahertz Electron. Conf., Darmstadt, Germany, Sept. 2829, pp. 5558 (2000).

[46] P. H. Siegel, A. Fung, H. Manohara, J. Xu, and B. Chang, "Nanoklystron: A monolithic tube approach to terahertz power generation." 12th Int. Space Terahertz Technol. Symp., San Diego, CA, pp. 8190 (2001).

[47] J. East and G. Haddad, "Ballistic tunneling transit time device for terahertz power generation." 12th Int. Space Terahertz Technol. Symp., San Diego, CA, pp. 6272 (2001).

[48] A. J. Deninger, T. Gobel, D. Schonherr, T. Kinder, A. Roggenbuck, M. Koberle, F. Lison, T. Muller-Wirts and P. Meissner, "Precisely tunable continuous-wave terahertz source with interferometric frequency control." Rev. Sci. Instrum. 79 044702 (2008).

[49] K.Kawase, M. Sato, T. Taniuchi and H. Ito, "Coherent tunable THz-wave generation from LiNbO3 with monolithic grating coupler." Appl. Phys. Lett. 68 24835 (1996).

[50] M. Kress, T. Loffler, S. Eden *et al.*, "Terahertz-pulse generation by photoionization of air with laser pulses composed of both fundamental and second-harmonic waves." Opt. Lett. 29 11202 (2004).

[51] G. A. Mourou, C. V. Stancampiano, A. Antonetti & A. Orszag, "Picosecond microwave pulses generated with a subpicosecond laser driven semiconductor switch." Appl. Phys. Lett. 39, 295296 (1981).

[52] G. Zhao, R. N. Schouten, N. van der Valk, W. T. Wenckebach & P. C. Planken, "Design and performance of a THz emission and detection setup based on a semi-insulating GaAs emitter." Rev. Sci. Instrum. 73, 17151719 (2002).

[53] N. Katzenellenbogen & D. Grischkowsky, "Efficient generation of 380 fs pulses of THz radiation by ultrafast laser pulse excitation of a biased metal- semiconductor interface." Appl. Phys. Lett. 58, 222224 (1991).

[54] Y. C. Shen, P. C. Upadhya, E. H. Linfield, H. E. Beere and A. G. Davies, "Ultrabroadband terahertz radiation from low-temperature-grown GaAs photoconductive emitters." Appl. Phys. Lett. 83 31179 (2003).

[55] M. Bass, P. A. Franken, J. F.Ward, & G. Weinreich, "Optical rectification." Phys. Rev. Lett. 9, 446448 (1962).

[56] X. F. Ma and X. C. Zhang, "Determination of ratios between nonlinear-optical coefficients by using subpicosecond optical rectification." J. Opt. Soc. Am. B, 10, 1175-1179 (1993).

[57] R. F. Kazarinov & R. A. Suris, "Possibility of the amplification of electromagnetic waves in a semiconductor with a superlattice." Sov. Phys. Semiconductors 5, 707709 (1971).

[58] J. Faist *et al.*, "Quantum cascade laser." Science 264, 553556 (1994).

[59] R. Kohler *et al.*, "Terahertz semiconductor-heterostructure laser." Nature 417, 156159 (2002).

[60] S. Kumar, "Recent progress in Terahertz quantum cascade lasers." IEEE J. Sel. Topics Quantum Electron., vol. 17, no. 1, pp. 3847, (2011).

[61] A. Bonvalet, M. Joffre, J. Martin & A. Migus, "Generation of ultrabroadband femtosecond pulses in the mid-infrared by optical rectification of 15 fs light pulses at 100 MHz repetition rate." Appl. Phys. Lett. 67, 29072909 (1995).

[62] Z. Huang and K. J. Kim, "Review of x-ray free-electron laser theory." Phys. Rev. ST Accel. Beams, 10, 034801 (2007).

[63] H. P. Freund and G. R. Neil, "Free-electron lasers: Vacuum electronic generators of coherent radiation." Proc. IEEE, vol. 87, no. 5, pp. 782803 (1999).

[64] B. W. J. McNeil & N. R. Thompson, "X-ray free-electron lasers." Nature Photonics. 4, 814821 (2010).

[65] B. S. Williams, "Terahertz quantum-cascade lasers." Nature Photonics. 1 51725 (2007).

[66] S. Fathololoumi, E. Dupont, C. W. I. Chan, Z. R. Wasilewsky, S. R. Laframboise, D. Ban, A. Matyas, C. Jirauschek, Q. Hu, and H. C. Liu, "Terahertz quantum cascade lasers operating up to $\sim$ 200 K with optimized oscillator strength and improved injection tunneling." Opt. Express 20, 3866 (2012).

[67] M. Razeghi, Q. Y. Lu, N. Bandyopadhyay, S. Slivken, Y. Bai, "Room temperature continuous wave THz quantum cascade laser source with high power operation." Proc. SPIE 9199, Terahertz Emitters, Receivers, and Applications V, 919902 (2014).

[68] B S. Williams, S. Kumar, Q. Hu & J. L. Reno, "High-power terahertz quantum cascade lasers." Electron. Lett. 42, 8991 (2006).

[69] Lianhe Li, Li Chen, Jingxuan Zhu, J. Freeman, P. Dean, A. Valavanis, A.G. Davies and E.H. Linfield, "Terahertz quantum cascade lasers with ¿1 W output powers." Electron. Lett. 50, 309311 (2014).

[70] A. Ashkin, "Acceleration and trapping of particles by radiation pressure." Phys. Rev. Lett. 24, 156 (1970).

[71] A. Ashkin, "Atomic-beam deflection by resonance-radiation pressure." Phys. Rev. Lett. 25, 1321 (1970).

[72] R. Scheider, H. Walther and L. Wöste, "Atomic beam deflection by the light of a tunable dye laser." Opt. Comm. 5, 337 (1972).

[73] T. W. Hansch and A. L. Schawlow, "Cooling of gases by laser radiation." Opt. Commun. 13, 68 (1975).

[74] D. J. Wineland and H. Dehmelt,"Proposed $10^{14}\delta\nu/\nu$ laser fluorescence spectroscopy on Tl^+ mono-ion oscillator III (sideband cooling)." Bull. Am. Phys. Soc. 20, 637 (1975).

[75] D. J. Wineland, R. E. Drullinger, and F. L. Walls, "Radiation-Pressure Cooling of Bound Resonant Absorbers." Phys. Rev. Lett. 40, 1639 (1978).

[76] W. D. Phillips and H. Metcalf, "Laser Deceleration of an Atomic Beam." Phys. Rev. Lett. 48, 596 (1982).

[77] S. Chu, L. Hollberg, J. E. Bjorkhlm, A. Cable and A. Ashkin, "Three-Dimensional Viscous Confinement and Cooling of Atoms by Resonance Radiation Pressure." Phys. Rev. Lett. 55, 48 (1985).

[78] J. Dalibard and C. Cohen-Tannoudji, "Laser cooling below the Doppler limit by polarization gradients: simple models." J. Opt. Soc. Am. B6, 2023 (1989).

[79] P. J. Ungar, D. S. Weiss, E. Riis, and Steven Chu, "Optical molasses and multilevel atoms: theory." J. Opt. Soc. Am. B6, 2058 (1989).

[80] David S. Weiss, Erling Riis, Yaakov Shevy, P. Jeffrey Ungar, and Steven Chu, "Optical molasses and multilevel atoms: experiment." J. Opt. Soc. Am. B6, 2072 (1989).

[81] A. Aspect, E. Arimondo, R. Kaiser, N. Vansteenkiste, and C. Cohen-Tannoudji,"Laser Cooling below the One-Photon Recoil Energy by Velocity-Selective Coherent Population Trapping." Phys. Rev. Lett. 61, 826 (1988).

[82] M. Kasevich and Steven Chu, "Laser cooling below a photon recoil with three-level atoms." Phys. Rev. Lett. 69, 1741 (1992).

[83] J. Lawall, S. Kulin, B. Saubamea, N. Bigelow, M. Leduc, and C. Cohen-Tannoudji, "Three-Dimensional Laser Cooling of Helium Beyond the Single-Photon Recoil Limit." Phys. Rev. Lett. 75, 4194 (1995).

[84] H. J. Lee, C. S. Adams, M. Kasevich, and S. Chu ,"Raman Cooling of Atoms in an Optical Dipole Trap." Phys. Rev. Lett. 76, 2658 (1996).

[85] H.J. Metcalf and P. Straten, "Cooling and trapping of neutral atoms." Phys. Rep. 244, 203 (1994).

[86] C.S. Adams and E. Riis,"Laser cooling and trapping of neutral atoms." Prog. Quant Electron, 21, 1 (1997).

[87] H.J. Metcalf and P. Straten, *Laser Cooling and Trapping*. (Springer, New York, 1999).

[88] M. Fox, *Quantum optics and introduction*. (Oxford University Press, Oxford, 2006).

[89] B.H. Bransden and C.J. Joachain, *Physics of atoms and molecules*. (Longman, Harlow, 1983).

[90] C.J. Foot, *Atomic Physics*. (Oxford University Press, Oxford, 2005).

[91] A. Einstein, "On the quantum theory of radiation." Physik. Zeit., 18, 121 (1917). Reproduced in English in P. Knight and L. Allen, *Concepts of quantum optics*. (Pergamon, Oxford, 1983).

[92] M. Fox, *Quantum optics and introduction*. (Oxford University Press, Oxford, 2006).

[93] M.O. Scully and M.S. Zubairy, *Quantum optics*. (Cambridge University Press, Cambridge, 1997).

[94] S. Hooker and C. Webb, *Laser Physics*. (Oxford University Press, Oxford, 2010).

[95] F. T. Arecchi and R. Bonifacio, "Theory of Optical Maser Amplifiers." IEEE J. Quantum Electron. 1, pp169-178 (1965).

[96] L. Mandel, "Sub-Poissonian photon statistics in resonance fluorescence." Opt. Lett. 4, 205 (1979).

[97] S. Stenholm, "The semiclassical theory of laser cooling." Rev. Mod. Phys. 58, 699 (1986).

[98] J. P. Gordon and A. Ashkin, "Motion of atoms in a radiation trap." Phys. Rev. A. 21, 1606 (1980).

[99] R. J. Cook, "Theory of resonance-radiation pressure." Phys. Rev. A. 21, 1078 (1980).

[100] C. Cohen-Tannoudji, "Laser cooling and trapping of neutral atoms: theory." Phys. Rep. 219, 153 (1992).

[101] Paul D. Lett, Richard N. Watts, Christoph I. Westbrook, William D. Phillips, Phillip L. Gould, and Harold J. Metcalf, "Observation of Atoms Laser Cooled below the Doppler Limit." Phys. Rev. Lett. 61, 169 (1988).

[102] M. Fox, *Quantum optics and introduction*. (Oxford University Press, Oxford, 2006).

[103] H. K. Onnes, "Further experiments with liquid helium. C. On the change of electric resistance of pure metals at very low temperatures, etc. IV. The resistance of pure mercury at helium temperatures." Commun. Phys. Lab. Univ. Leiden 120b (1911).

[104] H. K. Onnes, "Further experiments with liquid helium. D. On the change of electric resistance of pure metals at very low temperatures, etc. V. The disappearance of the resistance of mercury." Commun. Phys. Lab. Univ. Leiden 122b (1911).

[105] H. K. Onnes, "Further experiments with liquid helium. G. On the electrical resistance of pure metals, etc. VI. On the sudden change in the rate at which the resistance of mercury disappears." Commun. Phys. Lab. Univ. Leiden 124c (1911).

[106] H. K. Onnes, "Further experiments with liquid helium. H. On the electrical resistance of pure metals, etc. VII. The potential difference necessary for an electrical current through mercury below 4.19K." Commun. Phys. Lab. Univ. Leiden 133d (1913).

[107] D. Van Delft and P. Kes, "The discovery of superconductivity." Physics Today 63(9), 38 (2010).

[108] W. Meissner and R. Ochsenfeld, "Ein neuer Effekt bei Eintritt der Supraleitfa higkeit." Naturwissenschaften, 21, 787 (1933).

[109] F. London and H. London, "The electromagnetic equations of the supraconductor." Proc. Roy. Soc. (London), A149, 71 (1935).

[110] N. Ashcroft and D.Mermin, *Solid state physics*. (Brooks/Cole, Belmont, United States, 1976).

[111] M. Tinkham, *Introduction to Superconductivity*. (McGraw-Hill, Singapore, 1996).

[112] J. N. Rjabinin and L. W. Shubnikow, "Magnetic properties and critical currents of supraconducting alloys." Nature, 135, 581-582, (1935).

[113] V. L. Ginzburg and L. D. Landau, Zh, Eksperium. i Teor. Fiz. 20, 1064 (1950).

[114] W. S. Corak, B. B. Goodman, C. B. Satterthwaite, and A. Wexler, " Exponential temperature dependence of the electronic specific heat of superconducting vanadium." Phys. Rev. 96, 1442 (1954).

[115] W. S. Corak, B. B. Goodman, C. B. Satterthwaite and A. Wexler, " Atomic heats of Normal Superconducting Vanadium." Phys. Rev. 102, 656 (1956).

[116] R. E. Glover and M. Tinkham, "Transmission of superconducting films at millimeter-microwave and far infrared frequencies." Phys. Rev. 104, 844 (1956).

[117] R. E. Glover and M. Tinkham, "Conductivity of superconducting films for photon energies between 0.3 and $40kT_c$." Phys. Rev. 108, 243 (1957).

[118] L. N. Cooper, "Bound electron pairs in a degenerate Fermi gas." Phys. Rev. 104, 1189 (1956).

[119] J. Nagamatsu, N. Nakagawa, T. Muranaka, Y. Zenitani and J. Akimitsu, " Superconductivity at 39 K in magnesium diboride." Nature 410, 63 (2001).

[120] A. J. Leggett, "What DO we know about high T_c?." Nature Physics 2, 134 (2006).

[121] H. Takahashi *et al.*, "Superconductivity at 43 K in an iron-based layered compound $LaO_{1-x}F_xFeAs$." Nature 453, 376 (2008).

[122] J. R. Schrieffer and J. S. Brooks, *Handbook Of High-Temperature Superconductivity.* (Springer Science+Business Media.LLC, New-York, 2007).

[123] L. P. Gor'kov, "Microscopic derivation of the Ginzburg-Landau Equations in the theory of superconductivity." Sov. Phys.-JETP 9, 1364 (1959).

[124] A. A. Abrikosov, "On the magnetic properties of superconductors of the second group." Sov. Phys.-JETP 5, 1174 (1957).

[125] U. Essman and H. Träuble, "The direct observation of individual flux lines in type 2 superconductors." Phys. Lett. 24A, 526 (1967).

[126] H. F. Hess *et al.*, "Scanning-tunneling-microscope observation of the Abrikosov Flux Lattice and the Density of States near and inside a Fluxoid." Phys. Rev. Lett. 62, 214 (1989).

[127] H. F. Hess *et al.*, "Vortex-core structure observed with a scanning tunneling miccroscope." Phys. Rev. Lett. 64, 2711 (1990).

[128] P. W. Anderson, "The Resonating Valence Bond State in La_2CuO_4 and Superconductivity." Science 235, 1196 (1987).

[129] P. Monthoux, A. V. Balatsky and D. Pines, "Toward a Theory of High-Temperature Superconductivity in the Antiferromagneticaliy Correlated Cuprate Oxides." Phys. Rev. Lett. 67, 3448 (1991).

[130] M. Inui, S. Doniach, P. J. Hirschfeld, A. E. Ruckenstein, Z. Zhao, Q. Yang, Y. Ni, G. Liu, "Coexistence of antiferromagnetism and superconductivity in a mean-field theory of high-Tc superconductors." Phys. Rev. B 37, 5182 (1988).

[131] G. Kotliar and J. Liu "Superexchange mechanism and d-wave superconductivity." Phys. Rev. B 38, 5182 (1988).

[132] D. N. Basov and T. Timsuk, "Electrodynamics of high-T_c superconductors." Rev. Mod. Phys 77, 721 (2005).

[133] C. E. Gough *et al.*, "Flux quantization in a high-T_c superconductor." Nature 326, 855 (1987).

[134] V. J. Emery and S. A. Kiveison, "Importance of phase fluctuations in superconductors with small superfluid density." Nature 374, 434 (1995).

[135] T. Koyama and M. Tachiki, "I-V characteristics of Josephson-coupled layered superconductors with longitudinal plasma excitations." Phys. Rev. B. 54, 16 183 (1996).

[136] K. Tamasaku, Y. Nakamura and S. Uchida, "Charge dynamics across the CuO_2 planes in $La_{2-x}Sr_xCuo_4$." Phys. Rev. Lett 69, 1455 (1992).

[137] V. K. Thormsolle *et al.*, "C-axis Josephson plasma resonance observed in $Tl_2Ba_2CaCu_2O_8$ superconducting thin films by use of terahertz time-domain spectroscopy." Opt. Lett 26, 16 (2001).

[138] Sergey Savel'ev, V A Yampol'skii, A L Rakhmanov and Franco Nori, "Terahertz Josephson plasma waves in layered superconductors: spectrum, generation, nonlinear and quantum phenomena." Rep. Prog. Phys. 73, 026501 (2010).

[139] S. Sakai, P. Bodin and N. F. Pedersen, "Fluxons in thin-film superconductor-insulator superlattices." J. Appl. Phys 73, 2411 (1993).

[140] R. Kleiner and P. Müller, "Intrinsic Josephson effects in high-T_c superconductors." Phys. Rev. B 49, 1327 (1994).

[141] M. Machida, T. Koyama and M. Tachiki, "Dynamical Breaking of Charge Neutrality in Intrinsic Josephson Junctions: Common Origin for Microwave Resonant Absorptions and Multiple-Branch Structures in the I-V Characteristics." Phys. Rev. Lett 83, 4618 (1999).

[142] M. Machida and S. Sakai, "Unified theory for magnetic and electric field coupling in multistacked Josephson junctions." Phys. Rev. B 70, 144520 (2004).

[143] G. Binning and H. Rohrer, "Scanning tunneling microscopy." IBM. J. Res. Dev. 44, 1-2 (2000).

[144] B. D. Josephson, "Possible new effects in superconductive tunnelling." Physics Letters. 1, 251 (1962).

[145] P. W. Anderson and J. M. Rowell, "Probable observation of the Josephson superconducting tunneling effect." Phys. Rev. Lett. 10, 230 (1963).

[146] S. Shapiro, "Josephson currents in superconducting tunneling: The effect of microwaves and other observations." Phys. Rev. Lett. 11, 80 (1963).

[147] R. C. Jaklevic, John Lambe, A. H. Silver, and J. E. Mercereau, "Quantum interference effects in Jospehson Tunneling." Phys. Rev. Lett. 12, 159 (1964).

[148] V Bouchiat, D Vion, P Joyez, D Esteve and M H Devoret, "Quantum coherence with a single Cooper pair." Phys. Scr. T76, 165 (1998).

[149] Y.-F.Chen, D.Hover et al, "Micowave photon counter based on Josephson junctions." Phys. Rev. Lett 107, 217401 (2011).

[150] Xiao Hu and Shi-Zeng Lin,"Phase dynamics in a stack of inductively coupled intrinsic Josephson junctions and terahertz electromagnetic radiation." Supercond. Sci. Technol. 23, 053001 (2010).

[151] B. D. Josephson, "Coupled Superconductors." Rev. Mod. Phys. 36, 216 (1964).

[152] B. D. Josephson, "Supercurrents through barriers." Adv. Phys. 14, 419 (1965).

[153] R. P. Feynman, R. B. Leighton and M. Sands, *The Feynman lectures on physics*. (Addison-Wesley, Reading, Massachusetts 1966).

[154] V. Ambegaokar and B. I. Halperin, "Voltage due to thermal noise in the dc Josephson effect." Phys. Rev. Lett. 22, 1364 (1969).

[155] N. Martinov and N. Vitanov, "On some solutions of the two-dimensional sine-Gordon equation." J. Phys. A: Math. Gen. 25, 419 (1992).

[156] J. C. Eilbeck, P. S. Lomdahl and A. C. Newell, "Chaos in the inhomogeneously driven sine-Gordon equation." Phys. Lett. 87, 1 (1981).